

# Episodic venting of extreme subsalt overpressure through a thick evaporitic seal

Chris Kirkham<sup>a,\*</sup>, Joe Cartwright<sup>a</sup>, David James<sup>b</sup>, Luke Kearney<sup>a</sup>

<sup>a</sup> Department of Earth Sciences, University of Oxford, South Parks Road, Oxford, OX1 3AN, UK

<sup>b</sup> Cwmystwyth, Ceredigion, Wales, UK

## ARTICLE INFO

### Keywords:

Overpressure  
Pressure recharge  
Fluid escape pipes  
Episodic venting  
Salt  
Messinian salinity crisis  
Eastern Mediterranean  
Sedimentary basins

## ABSTRACT

Episodic venting from deep overpressured layers has rarely been documented in sedimentary basins, so the pressure evolution leading to these cyclical phenomena is poorly understood at present. Using three-dimensional (3D) seismic data from the West Nile Deep Sea Fan, we interpret >480 fluid escape pipes within a region of prolific leakage across a > 2 km thick sealing sequence of salt and claystones. Within this region, we map five linear trails of pipes with pockmarks or small mud volcanoes at their outlets and interpret them to have formed by episodic venting of overpressured fluids from beneath the salt, over a ~2–3 Myr period, coeval with basinward displacement of the pipes by flow of the salt. Importantly, the pipe trails root to the crests of stratigraphic traps at the base of the salt seal. Direct measurements from nearby exploration wells are used to construct pressure-depth and pressure-time plots over the lifetime of the pipe trails and demonstrate that overpressure near to or in excess of the lithostatic pressure must be repeatedly achieved in the stratigraphic traps to breach the salt seal every 50–150 kyrs. This pressure evolution is best described by a sawtooth pattern with overpressure relieved by venting, followed by re-seal of the trap, and pressure recharge. The pressure recharge for this episodic venting can most easily be explained here by biogenic gas generation and aquifer pressure transfer in the traps, with some minor contribution from sustained disequilibrium compaction during the Pliocene to Recent. The conditions necessary for this type of episodic venting should occur more widely, particularly in basins with thick evaporite deposits. The recognition of episodic venting has important implications for prospect de-risking, drilling safety and CO<sub>2</sub> and hydrogen storage.

## 1. Introduction

Venting of highly overpressured basinal fluids and gaseous hydrocarbons at the seafloor is increasingly recognized in many petroleum systems through the observation of localized fluid escape phenomena including mud volcanoes, gas chimneys and fluid escape pipes associated with surface pockmark arrays (Anderson et al., 2000; Judd and Hovland, 2009; Løseth et al., 2011; Stewart and Davies, 2006). Such phenomena are important to document and analyse, since they can provide important constraints on the distribution of overpressured compartments in a basin, and may provide evidence of secondary migration of hydrocarbons (Cartwright et al., 2007).

Most venting phenomena appear to represent a single, well defined episode of highly focused fluid escape to the sea floor. A good example is a single mud volcano, where the extrusion of a slurry of water and mud, commonly accompanied by gas, may erupt continuously or episodically

over a geologically short period of years to 1000s of years to build a single mud edifice (Deville et al., 2010). Much more rarely documented are venting phenomena that erupt from a single locus a number of times in a series of discrete fluid expulsion events, separated by long periods of dormancy. Vertically stacked pockmarks (Andresen and Huuse, 2011) or ‘Christmas tree’ mud volcanic structures are examples of these more long term episodic phenomena (Deville and Guerlais, 2009; Evans et al., 2007; Stewart and Davies, 2006). These episodic phenomena are important to understand more fully because they represent systems where a highly overpressured compartment of a basin is able to depressurize by venting some of the trapped overpressured fluids but is then subsequently re-pressured until a threshold is reached for another venting episode, leading to a ‘sawtooth’ pressure evolution through time (Cartwright et al., 2021). Analysis of this type of pressure evolution has the potential to shed light on specific overpressuring mechanisms in basins and on the temporal and spatial evolution of overpressured

\* Corresponding author.

E-mail address: [christopher.kirkham@earth.ox.ac.uk](mailto:christopher.kirkham@earth.ox.ac.uk) (C. Kirkham).

<https://doi.org/10.1016/j.marpetgeo.2022.105741>

Received 21 December 2021; Received in revised form 8 May 2022; Accepted 10 May 2022

Available online 16 May 2022

0264-8172/© 2022 The Authors. Published by Elsevier Ltd. This is an open access article under the CC BY license (<http://creativecommons.org/licenses/by/4.0/>).

compartments.

The aim of this paper is to reconstruct the pressure evolution of a group of recently discovered linear trails of fluid escape pipes that occur in a deep water setting in the Herodotus Basin on the lower continental slope off the West Nile Deep Sea Fan (Fig. 1) and discuss their implications for salt seal failure and pressure recharge. The pipe trails are located in an area where there has been active petroleum exploration involving both pre- and post-salt plays since the 1980s (Dolson, 2020; Gardosh and Tannenbaum, 2014), and where some >80 Tcf of gas has been discovered in the last decade (Cozzi et al., 2018; Dolson et al., 2005; Needham et al., 2017; Ratner, 2016).

Insights into the pressure distribution within this region are important not only for drilling safety, but from a wider context of understanding seals and migration (Dolson, 2020; Needham et al., 2017; Al-Balushi et al., 2016). It is commonly argued that thick evaporite layers represent almost ideal seals for petroleum entrapment because of their continuity, homogeneity and extremely low permeability (Downey, 1984). We show that the thick salt seal in the West Nile Deep Sea Fan has been repeatedly breached at 50–150 kys intervals above a suite of erosional stratigraphic traps at the base-salt. Furthermore, we show that the overpressure mechanisms operative in the basin during the Pliocene to Recent have been able to repeatedly recharge pressure in the stratigraphic traps to near or in excess of the lithostatic pressure.

## 2. Previous work

Several previous studies have documented linear pipe trails and have interpreted them as being related to episodic fluid escape from overpressured pre-salt traps, coeval to flow of the overlying salt layer through which the pipes propagate (Figs. 1 and 2) (Cartwright et al., 2018; Kirkham et al., 2019; Oppo et al., 2021b). These studies were all based on 3D seismic surveys located in the northern Levant Basin, offshore Lebanon (Fig. 1). They argued that the vented fluids were sourced from the crestal regions of folded and highly overpressured Oligo-Miocene reservoirs that are sealed by a ~1 km thick claystone layer that is overlain by the Messinian Evaporites (Fig. 2). The timing of venting was interpreted from the stratigraphic position of the outlet (pockmarks or mud volcanoes), and the pipes were interpreted to have formed by hydraulic fracturing of the thick salt and claystone seal (Cartwright et al., 2021; Kirkham et al., 2018b). The linear alignment of outlets is parallel with the regional salt flow direction. Importantly, their distribution was interpreted to be the result of episodic venting from the

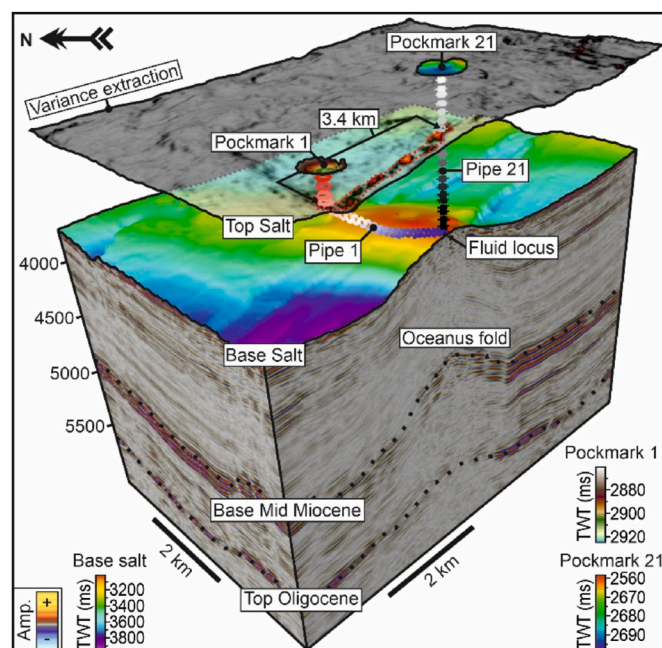


**Fig. 2.** A 3D model of the oldest and youngest fluid escape pipes and their genetically associated pockmarks outlets in a fluid escape pipe trail offshore Lebanon (modified from Cartwright et al. (2018); see Fig. 1 for location). The pipes emanated from the crest of a pre-salt fold in the Oligo-Miocene. The youngest pipe (Pipe 21) extends vertically through the Messinian Evaporites to a pockmark at the present-day seafloor. The oldest pipe in the trail (Pipe 1) has been deformed in the Messinian Evaporites by basinward flow of the salt unit. The post-salt and the pockmark therein for the oldest fluid escape pipe has been translated basinward by 3.4 km above the flowing salt.

crest of the pre-salt folded reservoir during regional basinward flow of the Messinian Evaporite. This resulted in offset of the outlet from above its genetically connected root in the pre-salt and deformation of the pipe in the salt (Fig. 2) (Evans et al., 2021; Kirkham et al., 2019). In this evolutionary model, each new venting episode forms a new vertical pipe by hydraulic fracture propagation through the salt and forms a new outlet at a younger stratigraphic position. The new pipe and outlet form in the same location as the preceding pipe and outlet that has since been offset from above the crest of the pre-salt fold by the flowing salt (Fig. 2). This makes interpreting each discrete venting episode relatively straightforward and negates the challenge of interpreting pockmark vents stacked within a pipes vertical zone of low signal-to-noise ratio (Andresen and Huuse, 2011).

Cartwright et al. (2021) demonstrated a method of using episodic fluid escape pipe trails located offshore Lebanon (Figs. 1 and 2) as a tool to assist in reconstructing overpressure magnitude and pressure evolution within a deeply buried overpressured compartment. Contrasting overpressuring mechanisms for episodic venting in this region have been proposed. Cartwright et al. (2021) argued that tectonic overpressuring is the dominant mechanism with a minor contribution from the buoyancy of a hydrocarbon column and disequilibrium compaction. In contrast, Oppo et al. (2021b) argued for lateral pressure transfer due to tilting of overpressured aquifers but with a minor contribution from tectonic compression as a possibility.

Most recently, Kirkham and Cartwright (2021) identified and mapped five linear fluid escape trails from a different basin in the Eastern Mediterranean (Fig. 1). This recent study was located in the Herodotus Basin in the area of the West Nile Deep Sea Fan (Figs. 1 and 3). The primary focus of that study was the identification of kinematic markers for the flow of the salt layer during salt tectonic deformation. The implications of these pipe trails for the pressure evolution of this area and cross-salt seal leakage was not considered. The purpose of this

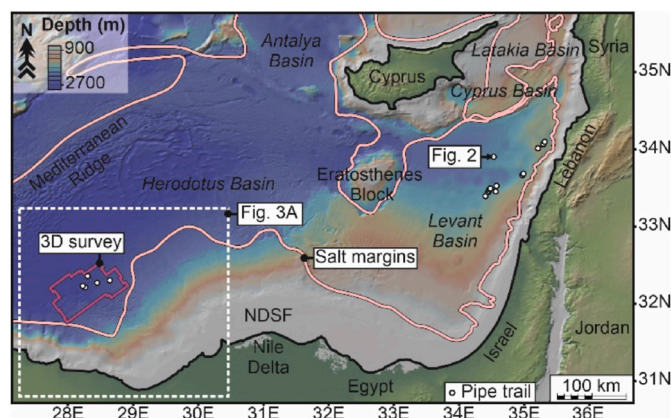


**Fig. 1.** Geographical setting of the Eastern Mediterranean. A bathymetric map in Eastern Mediterranean (from GeoMapApp [www.geomapp.org](http://www.geomapp.org)) showing the location of the various sub-basins, the margins of the salt basin (modified from Loncke et al. (2006) and Lofi et al. (2011)) and the location of the linear pipe trails identified in the northern Levant Basin and Herodotus Basin by Cartwright et al. (2018), Kirkham et al. (2019), Kirkham and Cartwright (2021) and Oppo et al. (2021b). NDSF – Nile Deep Sea Fan.



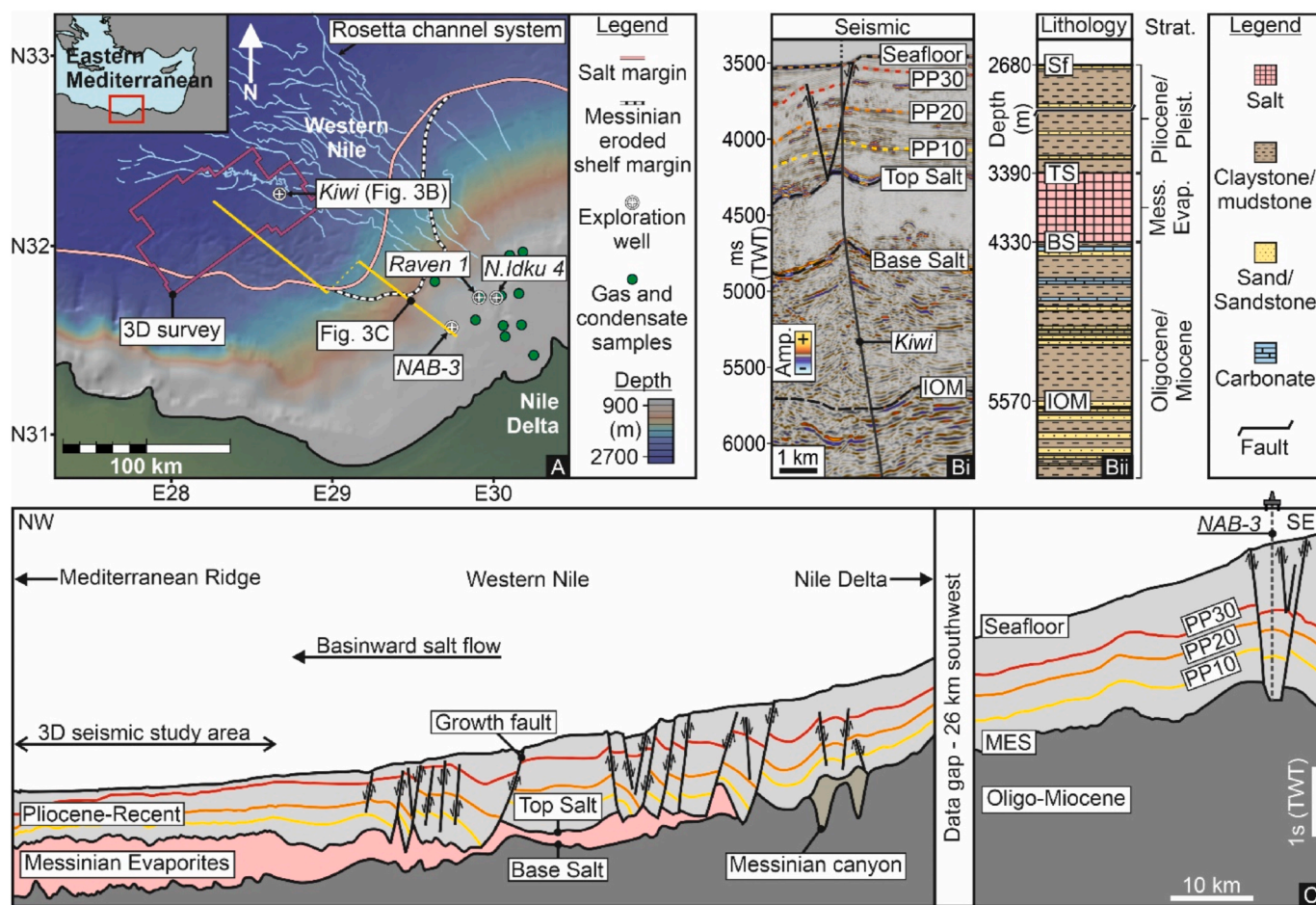


**Fig. 3.** Geological setting and stratigraphy of the western Nile and Deep Sea Fan. **A:** A bathymetric map of the western Nile (from GeoMapApp [www.geomapp.org](http://www.geomapp.org); see Fig. 1 for location) showing the location of the margins of the salt basin (modified from Loncke et al. (2006) and Lofi et al. (2011)), the Rosetta channel system (modified from Loncke et al. (2006)) and the location of gas and condensate samples from the Oligo-Miocene in the western Nile Delta (from Vandr  et al. (2007) and Halim et al. (1996)). The location of the 3D seismic survey and Kiwi, NAB-3, Raven 1 and N. Idku 4 exploration wells are shown. **Bi & Bii:** Seismic to proposed lithology tie in the study area (modified from Baer et al. (2016); see Fig. 3A for Kiwi well location). Sf – Seafloor, TS – Top Salt, BS – Base Salt, IOM – Intra-Oligo-Miocene. **C:** A regional cross-section (modified from Kirkham and Cartwright (2021)) extending from the Nile Delta across western Nile (see Fig. 3A for location). Key marker horizons calibrated at the NAB-3 well (see Gulmammadov (2017)) are correlated to the 3D seismic study area. MES – Messinian erosional surface.

manuscript is to explore the fluid plumbing system, pressure requirements, pressure evolution and overpressuring mechanisms for these episodic pipe trails. Whilst the episodic venting described here is comparable to the examples in the North Levant Basin in its expression as pipe trails, we show that the pipe trails in the West Nile Deep Sea Fan contrast in their trap configuration, source region, top seal and overpressuring mechanisms (see Section 6.2).

### 3. Geological setting and petroleum systems

#### 3.1. Geological setting

The study area is in the Herodotus Basin in the region of the West Nile Deep Sea Fan (Figs. 1 and 3A). The Nile Delta and Fan extend over a much older section of passive margin that formed following a period of rifting during the Jurassic to Early Cretaceous (Salem, 1976; Dolson et al., 2005). The Late Cretaceous to Mid Eocene period was dominated by carbonate deposition over much of the continental margin, with an almost complete lack of fluvial clastic input (Fig. 4) (Underwood et al., 2013). Uplift of East Africa during the Eocene triggered northerly drainage and a transition in the Mid-Late Eocene from carbonate to clastic deposition (Fig. 4).

The Oligo-Miocene succession contains a large volume of fluvial

sediments that prograded over the underlying carbonate platform and ramp (Figs. 3B, 4 and 5A) (Dolson et al., 2005; Said, 1962; Salem, 1976; Underwood et al., 2013). This succession is calibrated in the Raven and North Idku gas fields some 100 km east of the study area (Fig. 3A), where the Oligo-Miocene comprises marine shales with confined turbidites and multi-story channel systems (Fig. 4) (Kellner et al., 2018; Dolson, 2020).

Overlying the clastic wedge of the Oligo-Miocene, is the 1–1.5 km thick Messinian Evaporite sequence (Figs. 3B, 4 and 5A). This is primarily composed of halite and was deposited during the Messinian Salinity Crisis (~5.97–5.33Ma) (Krijgsman et al., 1999; Manzi et al., 2013; Meilijson et al., 2019) following a progressive disconnection of the Mediterranean Sea from the Atlantic Ocean. The Messinian Evaporites exhibit a wedge shaped geometry in the study area with a generally northward increase in thickness from a pinch out that runs along the basin margins (Figs. 1, 3 and 5A) (Hs  et al., 1977; Ryan, 2009). Immediately prior to salt deposition, the basin margins and some sections of the deeper basin were extensively incised by networks of valleys and submarine canyons that removed hundreds of meters of the Oligo-Miocene clastics (Bertoni and Cartwright, 2006; Druckman et al., 1995; Ryan and Cita, 1978; Mousoul t s et al., 2020). The rapid deposition of the thick salt layer (<500 Ka; Meilijson et al. (2019) and Roveri et al. (2014)) led to overpressuring of the Oligo-Miocene succession by undercompaction (Bertoni and Cartwright, 2015; Kirkham

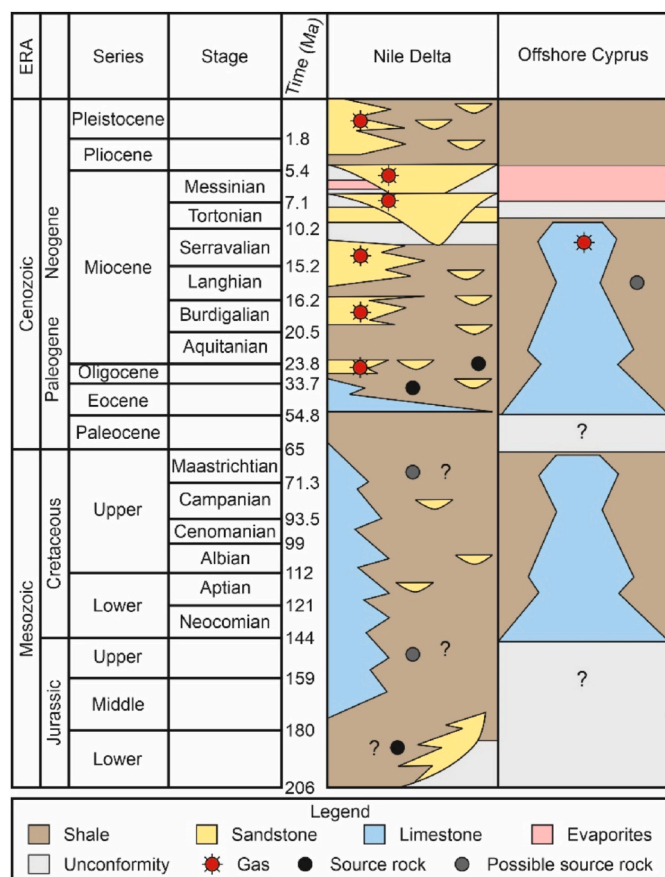


Fig. 4. Petroleum system of the Nile Delta and Offshore Cyprus (modified from Dolson (2020)).

et al., 2017; Al-Balushi et al., 2016). The Messinian Salinity Crisis was terminated by the Zanclean flood at 5.33 Ma when connection between the Atlantic Ocean and Mediterranean Sea was re-established (García-Castellanos et al., 2009).

The Pliocene to Recent period witnessed a return to clastic deposition in the basin with the development of the Nile Delta and Nile Deep Sea Fan (Figs. 3C and 4) (Loncke et al., 2006). The Pliocene to Recent stratigraphy is dominated by deep water hemipelagic deposits with turbiditic input to the study area via the Rosetta Canyon and Rosetta channel-levee system from the western branch of the Nile Delta (Loncke et al., 2004; Garziglia et al., 2008; Macgregor, 2012). Sedimentation rates of up to ~150 cm/kyrs are recorded for the Holocene close to the Rosetta Channel (Garziglia et al., 2008) and much lower rates of ~9 cm/kyrs from turbidites deposited over a mud volcano in the study area (Ducassou, 2006; Giresse et al., 2010).

Widespread basinward salt flow during the Pliocene to Recent has led to the development of an extensional domain with thinned salt and margin parallel normal faults that detach within the Messinian Evaporites, a translational domain containing little deformation, and a contractional domain with thickened salt, thrusts and salt cored folds that detach in the Messinian Evaporites (Allen et al., 2016). The study area straddles the extensional and translational salt tectonic domains, whereas the contractional domain is located further basinward toward the Mediterranean Ridge (Kirkham and Cartwright, 2021; Loncke et al., 2006). The simplest characterisation of the flow regime through the salt here is Couette flow although a more complex hybrid between Couette and Poiseuille flow is possible (Kirkham and Cartwright, 2021).

The West Nile Deep Sea Fan is one of the most prolific mud volcano provinces on Earth (Fig. 5B) (Kirkham et al., 2017). Giant mud volcanoes and mud canopies were extruded on top of the Messinian

Evaporites in the study area during the Late Messinian or Zanclean (Fig. 5) (Kirkham et al., 2018a, 2020b). These are amongst the largest mud extrusions on Earth and cover areas up to 300 km<sup>2</sup>, reach up to 1 km in thickness and are sourced from the Oligo-Miocene. A further >400 mud volcanoes (Fig. 5B) that are sourced from the Oligo-Miocene have erupted during the Early Pliocene to Present in the study area (Kirkham et al., 2017; Dupré et al., 2010; Loncke et al., 2004; Mascle et al., 2014).

### 3.2. Petroleum systems

The Nile Delta and Nile Deep Sea Fan is one of the major hydrocarbon provinces in the Eastern Mediterranean with estimated reserves of ~218 Tcf of gas and ~52 billion barrels of condensate (Hanafy et al., 2016; Dolson et al., 2014). The main reservoirs (mainly for gas) are Cretaceous-Miocene aged platform carbonates (Cozzi et al., 2018; Dolson, 2020) and slope channel sandstones of Oligo-Miocene and Pliocene age (Fig. 4) (Kellner et al., 2018; Dolson et al., 2005; Samuel et al., 2003). These reservoirs are sealed by marine shales and the regional Messinian Evaporites (Fig. 3) (Nashaat, 1994). The Messinian Evaporites seal Miocene Reservoirs with gas columns in excess of 600 m (Cozzi et al., 2018; Dolson, 2020).

The main source rocks are interpreted to be Pliocene sapropels, Oligo-Miocene pro-delta shales and Upper Cretaceous black shales (Fig. 4) (Aal et al., 2000; Dolson et al., 2005; Samuel et al., 2003; Vandr  et al., 2007; Sharaf, 2003). Geochemical analysis of gas samples from Early Miocene to Pliocene reservoirs in the western Nile Delta (Fig. 3A) are dominated by mixed microbial and thermogenic methane gas (Vandr  et al., 2007). Samples from mud volcanoes in the West Nile Deep Sea Fan (Fig. 5B) are strongly saturated with oily hydrocarbons (Pierre et al., 2014) and gas which has a mixed biogenic and thermogenic signature, with some high maturities indicative of seepage from great depth (Prinzhofer and Deville, 2013; Woodside et al., 2004). The basal Pliocene source interval is thermogenically immature throughout the Nile Delta, therefore these thermogenic gas seeps must be sourced from beneath the Messinian Evaporites (Aal et al., 2000; Sharaf, 2003; Vandr  et al., 2007). The Oligo-Miocene is a prolific biogenic source rock that has charged several large deepwater Oligo-Miocene discoveries in which >80 Tcf of methane has been discovered (Al-Balushi et al., 2016; Cozzi et al., 2018; Needham et al., 2017).

The region underlying the thick progradational packages of the Nile Delta is highly overpressured, with pressure increasing substantially beneath the Messinian (Dolson, 2020; Dolson et al., 2005). Overpressured gas condensate and reservoir water have been encountered in Miocene sandstones that are ~26–27.5 MPa above normal pressure conditions, with even higher pressures recorded in the overlying shales (Dolson, 2020; Heppard and Albertin, 1998). Highly overpressured non-commercial gas discoveries have also been made in Upper Oligocene slope channels (Dolson et al., 2005). The generation of these high pressures has been attributed to a combination of rapid sedimentation and sealing by the Messinian Evaporites, aquathermal processes, hydrocarbon generation and cracking of oil to gas in the lower Miocene to Upper Oligocene (Nashaat, 1994).

### 4. Data and methods

This study is based on the interpretation of a pre-stack time and depth migrated 3D seismic survey acquired in 2008 by Equinor over an area of 4300 km<sup>2</sup> of the West Nile Deep Sea Fan at water depths of 2500–3000 m (Figs. 1 and 3A). The data were acquired and processed with the objective of high-fidelity imaging of pre-salt exploration targets. Binset dimensions are 12.5 × 6.25 m, resulting in an effective lateral resolution of 25 m in the post-salt interval. Dominant frequencies in the pre- and post-salt intervals are 20 and 60 Hz, giving a vertical stratigraphic resolution of c. 40 m and 10 m, respectively. The data is processed to zero phase and displayed in SEG normal polarity (Brown, 2004), whereby an increase in acoustic impedance across an interface



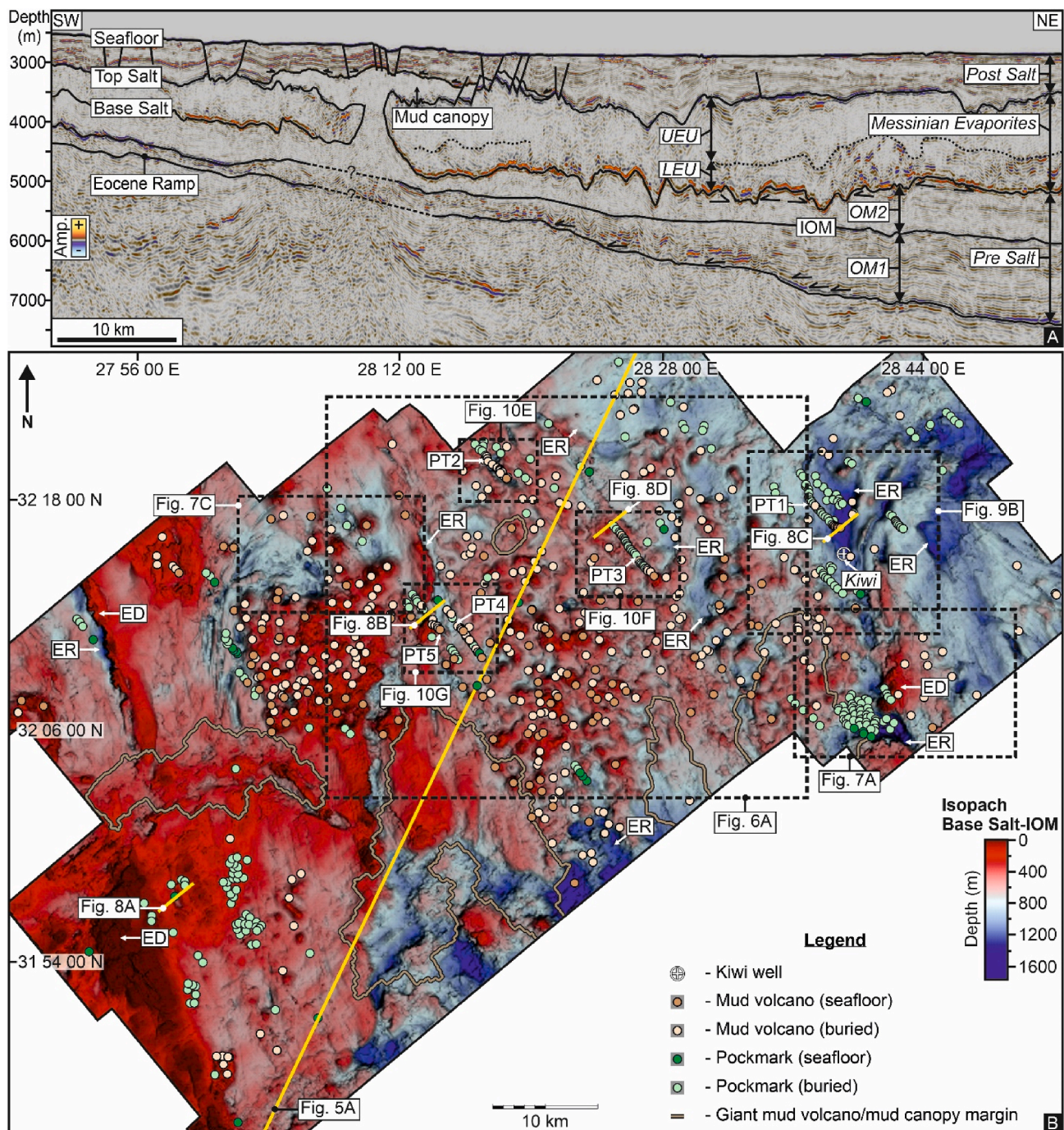


**Fig. 5.** Seismic stratigraphy, base salt structure and mud volcanoes, pipes and pipe trails in the study area. **A:** A seismic cross-section through the 3D seismic study area (see Fig. 5B for location) highlighting the key marker horizons and seismic stratigraphy. OM – Oligo-Miocene, IOM – Intra-Oligo-Miocene, LEU – Lower Evaporitic Unit, UEU – Upper Evaporitic Unit. **B:** IOM to Base Salt isopach map (see Fig. 3A for location) showing regional and anomalous thickness distribution of OM2 across the study area and erosional remnants (ER) and erosional depressions (ED). The location of all the mud volcanoes, pipes and 5 pipe trails (PT) are shown. The erosional remnants correlate with increases in thickness of OM2. The erosional depressions and also circular to elliptical mud depletion zones that underly the mud volcanoes correlate with decreases in thickness of OM2.

corresponds to a positive excursion on display. Accurate imaging of the Oligo-Miocene is hampered by a low signal-to-noise ratio, the occurrence of migration and transmission artefacts (Cartwright et al., 2021), multiples and converted wave interference patterns (Fig. 5A). These introduce some uncertainty into the interpretation of stratal geometries, particularly beneath features with pronounced relief at the base of the salt.

A number of key marker horizons (Fig. 3B and C) were manually picked and auto-correlated throughout the seismic survey area using

Schlumberger's Petrel software package. The regional horizons of PP10, PP20 & PP30 (3.22, 2.59 & 2.16 Ma respectively) were calibrated using high resolution biostratigraphic data from the NAB-3 exploration well located 100 km to the southeast of the study area (Fig. 3A and 3C) (Gulmammadov, 2017). Dating precision of this part of the geological time scale is considered to be within a single precession cycle i.e. c. 20 Ka. (Gradstein et al., 2012). However, we estimate the error in correlating these markers from the NAB-3 exploration well to the survey area as ~100 Kys based on an assessment of the uncertainty of seismic

correlation over the 100 km distance, and take this value as the error assigned to the dating of all the key marker horizons PP10, PP20 & PP30.

RMS (root-mean square) amplitude and coherency volumes were generated and interpreted following previously established criteria Cartwright and Santamarina (2015); Moss and Cartwright (2010a), to identify fluid escape pipes (referred to onwards as pipes) and their genetically connected outlets, and pipe trails (Fig. 2).

The onset of fluid venting in the pipe trails was established by dating the earliest pockmark or mud volcano (outlets) to form in each trail using dates for correlated marker horizons and extrapolation using average sedimentation rates (uncorrected for compaction). The ages of all subsequent outlets were calculated using the distance the outlet has been offset from the origin, with the origin being where the most recent outlet in the trail is situated (see section 2), divided by the average flow velocity of the salt. This average flow velocity was derived from the age of the outermost outlet and its distance from the origin (Fig. 2) (Kirkham and Cartwright, 2021). The average flow velocity of the salt is in the first instance assumed to be constant for the period represented by each pipe trail (see Discussion).

To quantify the pressure conditions required for the formation of the pipe trails, we constructed a series of pressure-depth plots for each trail (see Section 5.4 for detailed explanation). The hydrostatic and lithostatic gradients are calculated using the standard formula  $P = \rho \cdot g \cdot h$ , where  $P$  is pressure,  $\rho$  (rho) is the liquid or solid density,  $g$  is the acceleration of gravity and  $h$  is the height of the water or rock column. The hydrostatic gradient was calculated with a seawater density of 1.06 g/cc. The lithostatic gradient was calculated using bulk densities taken from nearby exploration wells for the Pliocene to Recent, Messinian Evaporites and Oligo-Miocene of 2.0, 2.13 and 2.35 g/cc, respectively. The fracture gradient for the salt was in the first instance assumed to be 2 MPa below the lithostatic pressure, based on arguments presented in Cartwright et al. (2021) in which the differential stress in the salt was taken as most likely to range between 1 and 3 MPa (Schoenherr et al., 2007; Weijermars and Jackson, 2014) and where the tensile strength was negligible. These values give a conservative estimate for the fracture gradient within the salt seal unit but significantly higher values are possible (see Discussion).

Pressure-depth plots for the first pipe that formed along the pipe trails are based on depth sections that are reconstructed to the stratigraphic configuration at the timing of the first venting episode. This requires removing an appropriate thickness of the younger overburden to restore the overburden thickness to the interval between the Top Salt and the first pockmark to form along the pipe trail. In the absence of any constraints on palaeo-water depth in the requisite time interval (4 Ma to Present), we assumed a constant water depth between reconstructed and present-day pressure-depth plots. Modest subsidence is implied by this assumption, and is supported by generally aggradational configurations of the shelf-slope depositional system updip from the study area (Allen et al., 2016; Loncke et al., 2006).

## 5. Results

### 5.1. Seismic stratigraphy

The seismic stratigraphy in the study area is divided here into three informal seismic stratigraphic units, the Pre-Salt (Pliocene-Recent succession), the Messinian Evaporites and the Post Salt (Oligo-Miocene succession). This subdivision is based on contrasts in seismic character, reflection geometries and well calibration and is described in detail below (Figs. 3B and 5A) (Baer et al., 2016).

#### 5.1.1. Pre Salt (Oligo-Miocene succession)

The Pre Salt has a wedge-shaped geometry and thins to the SW (Fig. 5A). This unit is sub-divided into two seismic-stratigraphic units, OM1 and OM2, based on contrasting seismic facies, reflection

geometrical relationships and gross unit geometry.

OM1 is the deeper of these units. The basal reflection of the unit is moderate to high amplitude, moderately continuous and is interpreted to represent the top of the Eocene carbonate ramp (Fig. 5A). OM1 is composed of moderate amplitude and parallel reflections that gently dip toward the SE and are divergent to the geometry of the Eocene ramp (Fig. 5A). OM1 reaches thicknesses of 1800 m in the deep basin to the north and thins onto the Eocene ramp to as little as 200 m with some evidence of onlap onto the slope (Fig. 5A). The lithology of OM1 is probably composed of marine shales and sandstones confined in stacked channel systems and basin floor fans (Figs. 3B and 4). This sub-unit is host to several extensive and localised high amplitude anomalies that display a gradual reduction in amplitude toward their margins, are an enhancement of reflections with no phase reversal and are not underlain by any velocity artefacts (Fig. 6). Amplitude window extractions at the base of OM1 show large anomalies that are distributed N-S and reach up to ~20 km in width (Fig. 6A and B). Amplitude window extractions through some shallower anomalies in OM1 are oriented NNW-SSE/NW-SE, up to 3 km wide and display sinuosity in the amplitude distribution (Fig. 6C-E). We interpret these amplitude extractions as Oligocene submarine fan (Fig. 6A) and channel (Fig. 6C) sandstone reservoirs.

The base of OM2 (top of OM1) is characterised by a transition toward low amplitude to transparent seismic reflections (Fig. 5A). The lithology of OM2 is dominated by shales (Figs. 3B and 4), which provide the mud source for the hundreds of mud volcanoes in this study area (Fig. 5) (Kirkham et al., 2017). OM2 is bound at its top by the regionally correlatable, high amplitude and acoustically 'soft' reflection of the Base Salt (Figs. 3B and 5A). Some moderate amplitude, parallel and more continuous reflections can be interpreted within the otherwise low coherency unit that are concordant to the reflections in OM1 and discordant to the Base Salt (Fig. 5A). There are no amplitude anomalies in this unit that would be indicative either of significant reservoirs or gas accumulations (Fig. 6B, D, E).

OM2 generally thickens eastwards across the study area from c. 200 m to >1000 m (Fig. 5B), but with numerous areas of locally increasing and decreasing thickness that correlate with highs or lows at the Base Salt. The relief on these highs at the Base Salt is up to 1 km with geometries that form plateaux and generally N-S oriented ridges (Figs. 5B, 7A and 7B). The ridges are separated by linear troughs at the Base Salt, that coincide with thinning of OM2 to <100m (Figs. 5, 7A and 7B). Along the flanks of these ridges, the Base Salt subtends angles of between 3 and 38° relative to the more coherent truncated reflections of OM2, implying significant degrees of erosional relief of up to 1000 m (Figs. 5A and 7B). These N-S depressions or troughs are interpreted as incised valleys or submarine canyons that were cut during the major lowstand at the onset of the Messinian Salinity Crisis and are analogous to similar features mapped further east beneath the Nile Delta (Barber, 1981).

Another set of features that can be seen on the Base Salt are a series of prominent circular-elliptical depressions up to a few km across (Figs. 5B, 7C and 7D). These coincide with localized thinning of OM2 and have been interpreted previously as mud volcano depletion zones that formed during the remobilization of mud from OM2 and extrusion at contemporaneous seafloors throughout the Pliocene-Recent (Kirkham and Cartwright, 2021; Kirkham et al., 2017).

#### 5.1.2. Messinian Evaporites

The top of the Messinian Evaporites is represented by the regionally correlatable, high amplitude and acoustically 'hard' seismic reflection of the Top Salt (Figs. 3B and 5A). The Messinian Evaporites are divided into two sub-units in the study area, a Lower Evaporitic Unit and Upper Evaporitic Unit, based on contrasts in seismic facies and reflection geometry and continuity (Fig. 5A). The Lower Evaporitic Unit is composed of discontinuous and high amplitude reflections interbedded with seismically transparent layers (Fig. 5A). The top of the Upper Evaporitic Unit is discontinuous and represented by a seismic facies transition to almost entirely seismically transparent Upper Evaporitic Unit (Fig. 5A).



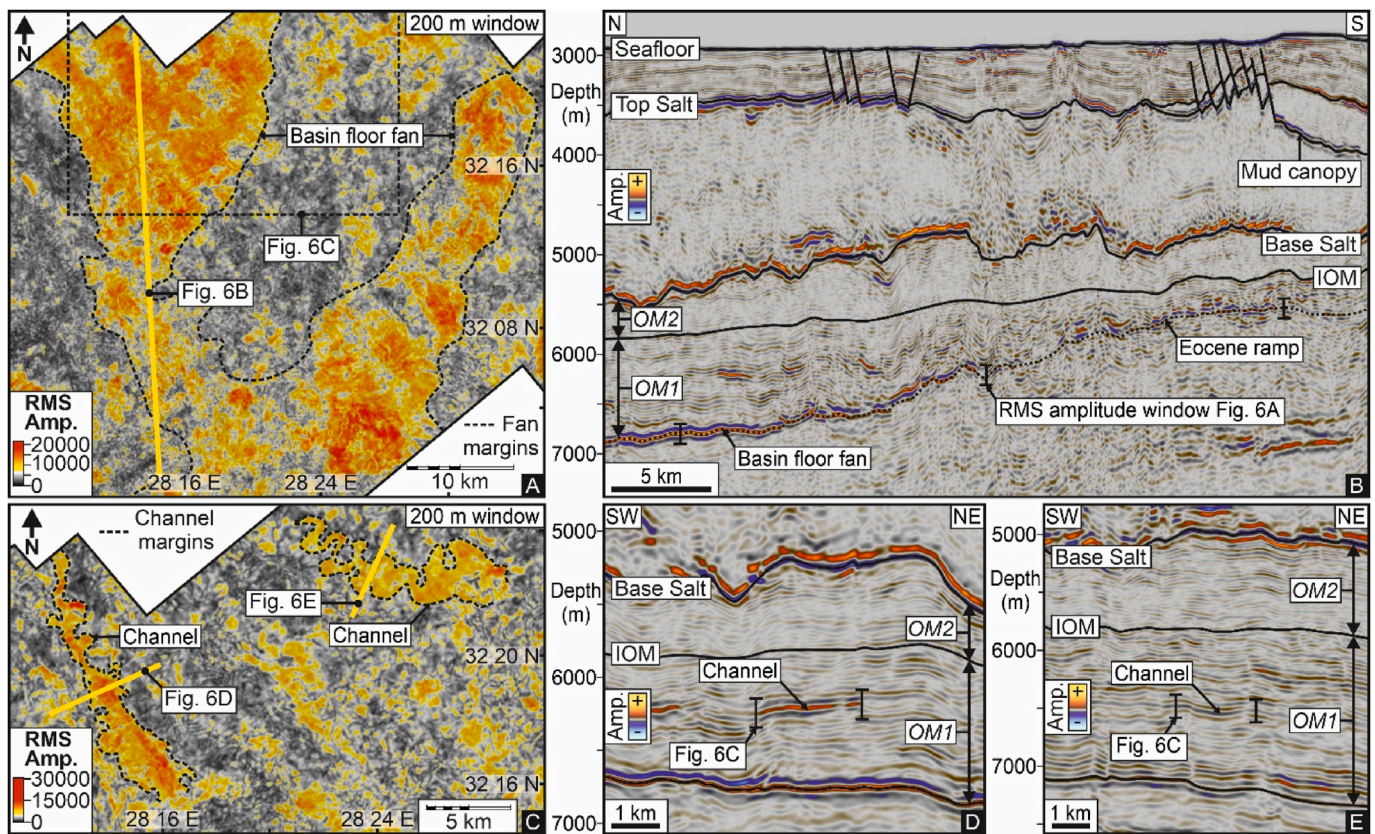


**Fig. 6.** Amplitude anomalies in the Pre Salt. **A:** A 200 m RMS amplitude window map (see Fig. 5B for map location and Fig. 6B for window position) covering a set of 'hard' amplitude anomalies at the base of OM1 overlying the Eocene carbonate ramp that are orientated N-S and interpreted as basin floor fans. **B:** A seismic cross-section (see Fig. 6A for line location) highlighting the extensive high amplitude basin floor fan overlying the Eocene ramp. OM1 contains several high amplitude anomalies while OM2 is comparatively featureless. **C:** A 200 m RMS amplitude window map (see Fig. 6A for map location and Fig. 6D for window position) through a set of localised high amplitude anomalies in OM1 that are oriented NW-SE that display sinuosity in planform and are interpreted as submarine channels. **D & E:** Seismic cross-sections (see Fig. 6C for line locations) showing the localised and high amplitude seismic character of the channels shown in Fig. 6C. OM2 contain no clear amplitude anomalies in contrast to OM1. OM – Oligo-Miocene; IOM – Intra-Oligo-Miocene.

The contrast in seismic facies between the Upper and Lower Evaporitic Units is attributed to the inclusion of thin clastic layers interbedded in the Lower Evaporitic Unit (Kirkham et al., 2020a; Kirkham and Cartwright, 2021). Long range correlation of these two sub-units to the Levant Basin suggests that the Lower Evaporitic Unit is the lateral equivalent of the reflective intra-salt series in the Levant Basin (ME I–V (Kirkham et al., 2020a; Hübscher et al., 2007)). The intra-salt reflections in the Levant Basin are equated to thin (1–3 m) layers of diatomaceous claystones interbedded in a dominantly halite succession (Feng et al., 2017; Meilijson et al., 2019). Locally, the Messinian Evaporites thin overlying the erosional highs between the palaeo-valleys and canyons at the Base Salt (Fig. 7B). This thinning is primarily within the Lower Evaporitic Unit (Fig. 7B). Juxtaposition of the Messinian Evaporites with the erosional highs at the Base Salt presents the potential for well-sealed stratigraphic traps (palaeogeomorphic traps).

#### 5.1.3. Post Salt (Pliocene to recent succession)

The Post Salt Unit in the study area is located within the distal part of the Nile Deep Sea Fan where sediment deposition is mostly aggradational within a deep-water slope setting (Fig. 3A, C and 5A). It is dominated by laterally continuous and moderate to high amplitude reflections but with local interbedding of channels, channel-levees, and mass transport deposits (Figs. 3B and 5A). The Rosetta Channel cuts across the northeast of the study area, and is prominent at the modern seafloor (Fig. 3A). The Post Salt is deformed by an array of growth faults in the south (Fig. 5A) and these form part of the circum-basin margin growth fault belt, at the head of the extensional domain that developed

in response to gravity tectonics from the Late Pliocene onwards (Kirkham et al., 2017; Loncke et al., 2006; Allen et al., 2016). Increased proximity to the western Nile and sediment transport from the Rosetta Channel has led to thickening of the Post Salt (Fig. 3C) from ~500 to 1000 m toward the east of the study area. Nearly 400 mud volcanoes are interpreted within the Post Salt and are all sourced from OM2 (Fig. 5B).

## 5.2. Evidence for fluid escape

### 5.2.1. Pipes and pockmarks

We mapped 382 individual fluid escape pipes with single pockmarks at their outlets in the study area. They are spatially distributed throughout the study area (Fig. 5B) and temporally distributed at several stratigraphic levels from the Early Pliocene to Recent (Fig. 8). The pockmarks exhibit classic crater geometry, with excavated relief of 10–50 m and diameters of 70–500 m (Fig. 8A). The pipes that terminate upwards at these pockmarks transect both the Post Salt and the Messinian Evaporites (Fig. 8A) (c.f. Kirkham et al. (2018b)). They cannot easily be traced below the Base Salt (Fig. 8). Amplitude anomalies are frequently observed overlying and adjacent to these pipes and pockmarks (Fig. 8A–C). They have a 'soft' acoustic response, typically display a phase reversal and a strong anomalous amplitude relative to the host stratigraphy with sharp lateral cut-offs of amplitude (Fig. 8B). They are directly underlain by vertical zones of amplitude attenuation and push-down (Fig. 8B). These characteristics lead us to interpret the amplitude anomalies as due to shallow gas (Løseth et al., 2009; Hammond, 1974).



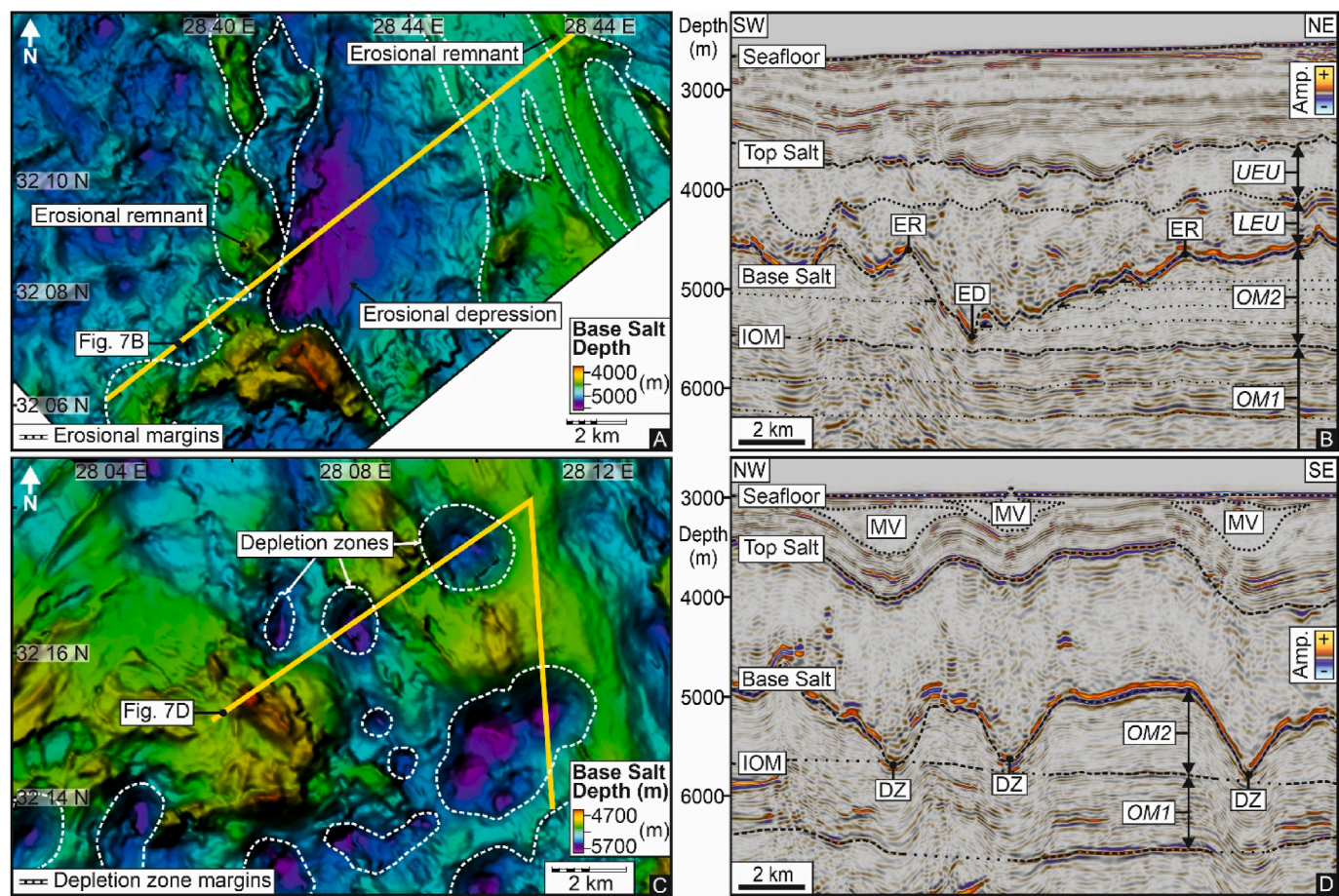


**Fig. 7.** Base Salt character, erosion and mud depletion. **A:** A depth map of the Base Salt (see Fig. 5B for location) showing erosional remnants that are orientated N-S/NNW-SSE and erosional depressions adjacent. **B:** A seismic cross-section (see Fig. 7A for location) showing the erosional character of the Base Salt, with ~1000 m of truncation of OM2 into the erosional depression (ED) and erosional remnants (ER) with large structural relief. The Messinian Evaporites thicken into the depression and the Top Salt is discordant with the Base Salt. LEU – Lower Evaporitic Unit, UEU – Upper Evaporitic Unit, OM – Oligo-Miocene, IOM – Intra-Oligo-Miocene. **C:** A depth map of the Base Salt (see Fig. 5B for location) showing the circular to elliptical depressions of depletion zones formed during mud volcanism. **D:** A seismic cross-section (see Fig. 7C for location) showing the localised bowl-shaped depressions at the Base Salt and thinning of OM2 associated with the mud depletion zones. The depletion zones (DZ) are directly overlain by mud volcanoes (MV) in the Post Salt and the Top Salt shows some concordance with the Base Salt overlying the depletion zones.

The majority of the 382 pipes mapped in the study area are associated with palaeo-pockmarks signifying that the pipes formed at some time in the Pliocene to Pleistocene (Fig. 8A and D). These older pipes have been deformed by basinward flow of the salt and hence their pockmark outlets are offset a substantial distance from their original expulsion locus. This means that the locus for the fluid expulsion cannot be identified with certainty. However, a small minority (24) of pipes are associated with pockmarks at the present-day seafloor (Figs. 5B and 8A). These have not been offset from their expulsion locus, and it is possible to identify with certainty that these pipes all root to erosional stratigraphic traps at the Base Salt (Figs. 5B, 7B and 8A). These stratigraphic traps have structural relief ranging from 70 to 500 m in magnitude (~350 m on average). The erosionally truncated stratigraphy of OM1 and OM2 forming the stratigraphically trapped rock volume is parallel stratified and gently dipping (Figs. 5A, 7B and 8A). Since the 24 fluid escape pipes root to the crests of the stratigraphic traps at the base of the main seal (the Base Salt), we consider that it is the pressure within the uppermost unit juxtaposed against the Base Salt (i.e. OM2) that must be responsible for the fluid leakage. Since fluid escape pipes have been previously equated with hydraulic fracturing, we can also infer that the critical pore fluid pressure condition for pipe formation is met at the crest of these stratigraphically trapped compartments of the OM2 Unit.

### 5.2.2. Pipe trails

Five separate pipe trails (PT1-PT5; Figs. 9 and 10) have been identified and mapped in the study area in a previous study in an attempt to constrain the salt kinematics in the area (Kirkham and Cartwright, 2021). Their seismic characteristics are only briefly summarised here since our emphasis in this study is to use the trails to analyse the episodicity of the fluid escape phenomena.

All 5 pipe trails are all located within the translational domain of the salt basin where there is little contraction or extension and the salt thickness is assumed to have been conserved (Kirkham and Cartwright, 2021). The Post Salt has been translated here by the northwesterly flow of the underlying Messinian Evaporites.

The development of the pipe trails has been interpreted as due to episodic venting from an underlying highly overpressured source interval, across the Messinian Evaporites but where each pipe and pockmark is passively translated down the salt flow direction (Kirkham and Cartwright, 2021). The most recently formed outlet in each pipe trail is positioned at the Seafloor above the crest of a Base Salt fluid expulsion locus (Figs. 8C and 9A). The oldest pipe and outlet in each pipe trail (Pipe 1) also originally formed above the crest of these same Base Salt fluid expulsion loci, but have been offset to the northwest by translation of the Post Salt during salt tectonic deformation (see section 2).

Trails PT1-PT5 are all mapped as NW-SE trending linear alignments



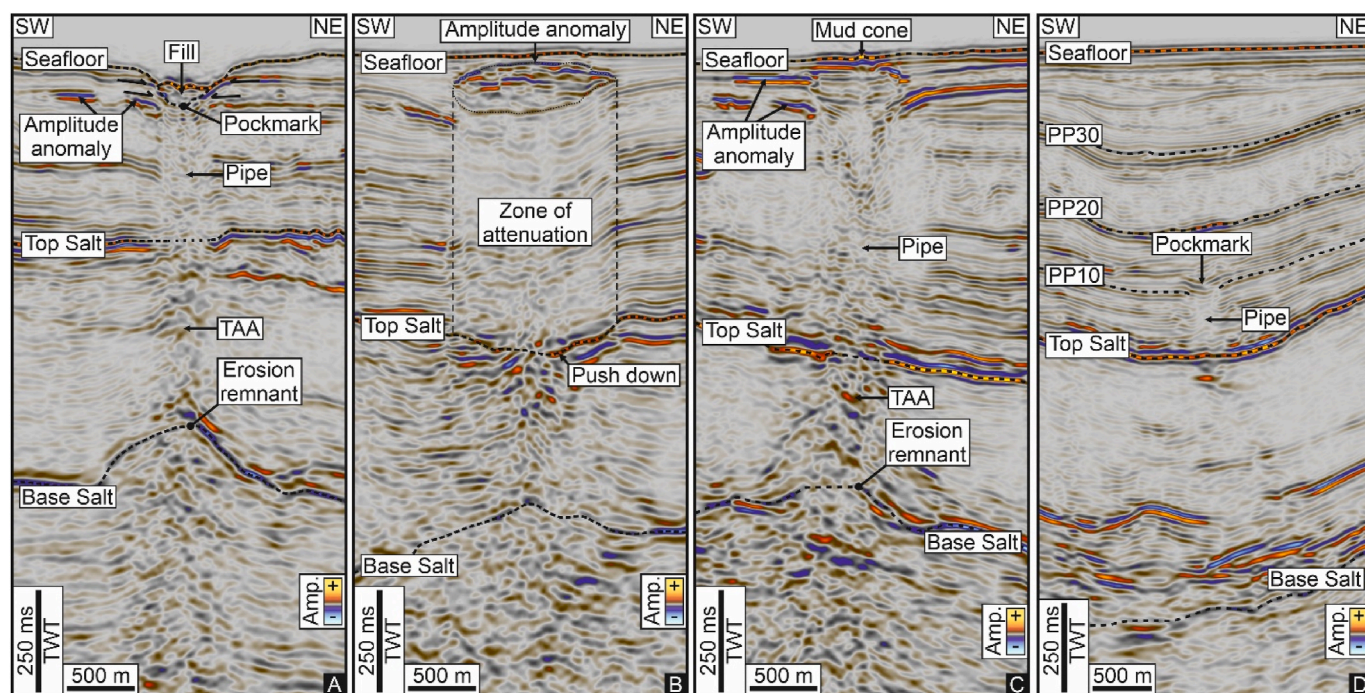


**Fig. 8.** Pipes and shallow gas amplitude anomalies. **A:** A seismic cross-section (see Fig. 5B for location) showing a pipe emanating from a stratigraphic trap (erosional remnant) at the Base Salt. The outlet for the pipe is a pockmark at the seafloor that truncates shallow reflections in the Post Salt. Shallow 'soft' amplitude anomalies are present adjacent to the pipe. TAA – Trail of amplitude anomalies. **B:** Shallow gas adjacent to a set of pipes producing a high amplitude anomaly (see Fig. 5B for location). The amplitude anomaly has a 'soft' top, abrupt amplitude cut-off at its margins and is underlain by a vertical zone of amplitude attenuation and push down. **C:** A seismic cross-section through the youngest pipe in PT1. Its outlet is a small mud cone at the seafloor (see Fig. 5B for location). **D:** A seismic cross-section through the oldest pipe in PT3. Its outlet is a deeply buried pockmark (see Fig. 5B for location).

of pockmarks or small mud cones at the outlet to each pipe (Figs. 5B, 9 and 10). The pockmark or mud cone outlets (Fig. 8C and D) young successively in a south-easterly direction towards the locus of eruption (Figs. 9 and 10). The vertical spacing between outlets is relatively continuous in PT2-5 resulting in a gradual shallowing in the stratigraphic position of each successive outlet (Fig. 10A–D). The four most recent outlets in PT1 shallow more acutely due to an increase in sedimentation rate resulting from a shift in the Rosetta channel system in the later Pleistocene (Fig. 9A). The base of outlets 9 and 10 in PT1 are positioned at greater depths than the immediately preceding outlets due to the erosional relief of the pockmarks and local collapse within the pipes vertical zone (Fig. 9A). The pipe trails are poorly imaged in the Messinian Evaporites, with only stacked amplitude anomalies serving to indicate their presence.

The early stages of fluid venting in PT1 differs from the other pipe trails in that it is expressed in the form of a dissolution structure in the Post Salt (Fig. 9). This dissolution structure has been interpreted by Kirkham and Cartwright (2021) to have been displaced 5130 m NW away from the crest of the Kiwi High at the Base Salt by the flowing salt and to have formed via subjacent dissolution at the crest of the Kiwi High (Fig. 9).

**5.2.2.1. Dating the fluid expulsion episodes.** The pipe trails were dated by correlation of each outlet horizon to the chronostratigraphic framework provided by the regionally correlated and age calibrated marker horizons (Fig. 3C; see data and methods). The age of the oldest pipe varies from trail to trail; the oldest is dated as  $3.3 \pm 0.1$  Ma in PT3 (Fig. 8D) (Table 1). In each of the five pipe trails, the youngest pipe to form terminates at an outlet at the present-day seabed, implying that leakage has occurred geologically very recently in each case, possibly within the Holocene (Figs. 9A and 10A–D).

The distance from the oldest to youngest (present day) outlet in each pipe trail (Figs. 9 and 10) records the translation distances of the flowing

salt layer during the time interval of episodic venting through successive pipes in each trail. These translation distances differ from trail to trail because their overall longevity and the local salt flow velocity varies. The translation distances for the five trails range from 3830 to 6330 m, yielding time averaged flow velocities ranging from  $1.7 \pm 0.3$  to  $2.6 \pm 0.3$  mm/a (Table 1) (Kirkham and Cartwright (2021)).

The timing of venting episodes and duration of time between venting episodes varies from trail to trail (Fig. 11). Comparisons from trail to trail are facilitated and constrained by high confidence seismic correlation of the PP30 and PP40 horizons in a transect that links all five trails (Figs. 9A and 10A–D). Mapping of these horizons throughout the study area provides an additional two absolute chronostratigraphic markers to correlate groups of pipe outlets from trail to trail, in 'windows' of time (T1 and T2 in Fig. 11) that can be confidently equated from trail to trail. The PP30 horizon is biostratigraphically calibrated ( $2.16 \pm 0.1$  Ma), whereas the PP40 horizon is not. Dates given for the oldest outlet in the pipe trails are based on average sedimentation rates referenced to the markers with known ages. The age of the other outlets in the pipe trails is based on the translation distance and velocity. PT1-3 show a good correlation between the age calibrated horizon of PP30 and relative dated horizon of PP40 and the outlet dating utilising average salt flow (see methods; Fig. 10). PT4 & PT5 however show mismatches in the timing of PP30 and dating using average flow velocity (Fig. 10). This suggests some localized variability in translation velocity of the Post Salt during the lifetime of PT4 & PT5.

The total number of venting episodes per trail ranges from 13 to 27 (Table 1). This is partly due to different longevity of each trail. PT2, 4 & 5 have similar onset timings ( $2.2 \text{ Ma} \pm 0.1 \text{ Myrs}$ ). The number of venting episodes during each time window also varies. Note for example the contrasts in PT2, 3 & 5 during window T1 (Fig. 11). During window T2, there are contrasting numbers of episodes for all five trails (Fig. 11). There is no convincing evidence for synchronicity in venting from trail to trail. They appear to exhibit independent fluid expulsion histories.



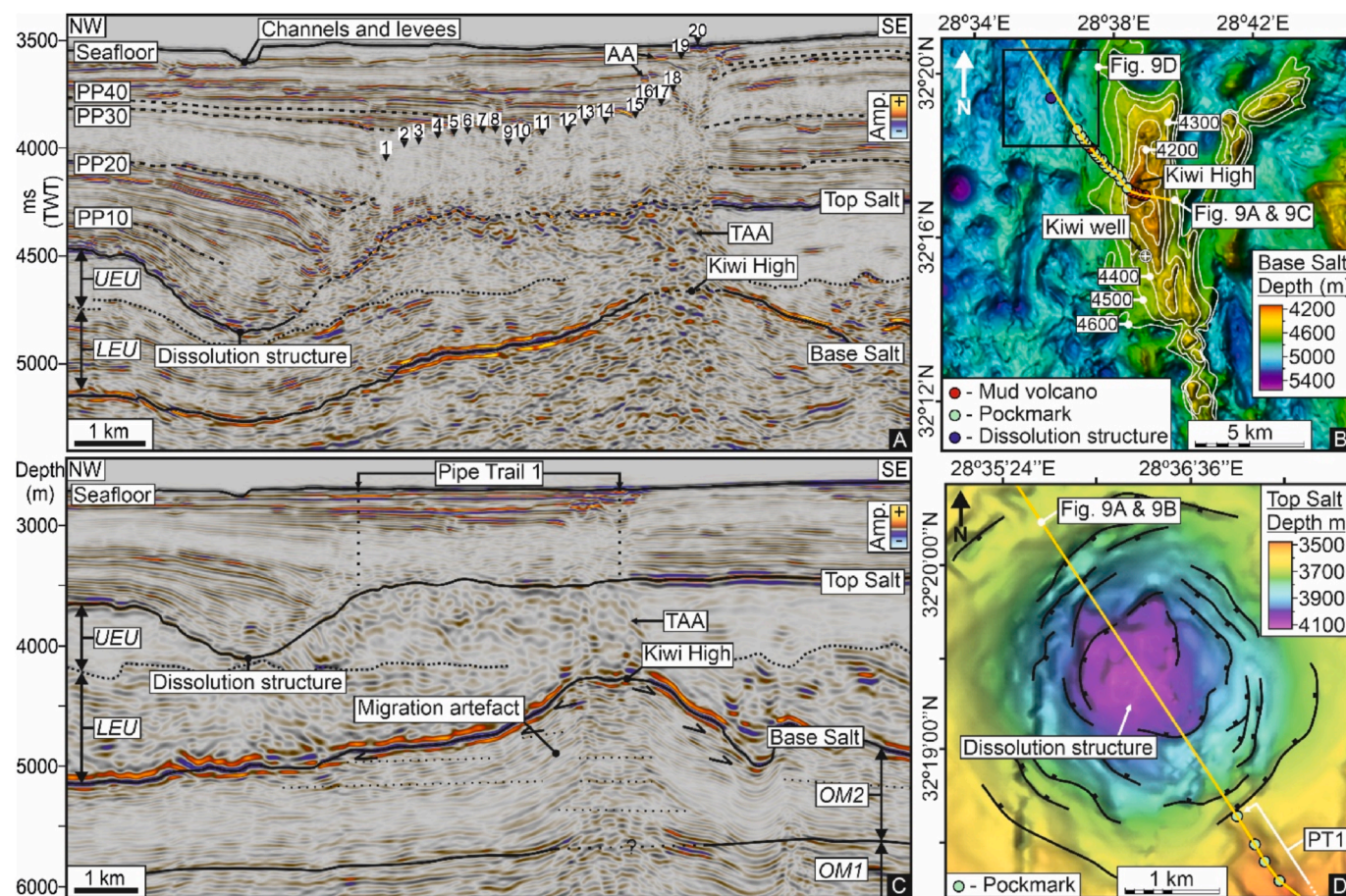


**Fig. 9.** Episodic venting in Pipe Trail 1 (PT1), sourced from the Kiwi High. **A:** A Two-way time seismic cross-section (modified from Kirkham and Cartwright (2021); see Fig. 9B for location) through PT1 and the Kiwi High. The outlets for the pipes systematically young to the SE. Their order of formation is numbered. The labels point to the base of the outlets. The most recent pipe emanates from the crest of the Kiwi High at the Base Salt and has an outlet at the present seafloor. 'Soft' amplitude anomalies (AA) are distributed adjacent to the pipe outlets. A dissolution structure is located to the NW of pipe 1 in the trail. The Upper Evaporitic Unit (UEU) thins beneath the dissolution structure and the Lower Evaporitic Unit (LEU) thins onto the Kiwi High. TAA – Trail of amplitude anomalies. **B:** A depth map of the Base Salt (modified from Kirkham and Cartwright (2021); see Fig. 5B for location) and structure contours over the Kiwi High. The most recent pipe is positioned above the crestal region of the Kiwi High. **C:** A depth seismic cross-section (same line of section as Fig. 9A) showing the significant structural relief of the Kiwi High. The stratigraphy in OM1 and OM2 is parallel stratified and truncated against the Base Salt margins of the Kiwi High, similar to other erosional remnants in the study area (see Fig. 7B). Numerous migration artefacts are superimposed over the true stratigraphy. OM – Oligo-Miocene. **D:** A depth map of the Top Salt (modified from Kirkham and Cartwright (2021); see Fig. 9B for location) showing the bowl-shaped depression of the dissolution structure.

All five pipe trails exhibit contrasts in the range and average horizontal spacing between pipes, as well as the time range and average time between venting episodes (Table 1). The majority of intervals between venting episodes fall in the range 50–150 Ka (Fig. 12). There is no systematic relationship between outlet type, erosional relief of the outlets and outlet spacing (Fig. 11).

**5.2.2.2. The root zone for the pipe trails.** The locus for seal breach for four of the five pipe trails (PT1, 2, 4 & 5) is similar to that found for the 24 single pipes i.e. a crestal position defined by the depth map of the Base Salt (Figs. 9 and 10). It was not possible to establish the original expulsion locus of PT3, simply because the last expulsion episode extruded a large mud volcano at the present-day seafloor, and the depletion zone associated with this event profoundly altered the Base Salt configuration. Since PT3 is located close to a prominent Base Salt erosional ridge (Fig. 10B and F), we suspect that it, too, emanated from a crestal position at the Base Salt.

In contrast with the examples of the 24 individual pipes (Fig. 8A), the roots of the pipe trails are much larger relief features, with structural relief to potential spill of a truncation trap ranging from 520 to 830 m (Figs. 9 and 10). The largest of these is the Kiwi High which forms the root for PT1 (Fig. 9). OM2 defines the stratigraphic trap configuration

within the Kiwi High with a top and lateral seal provided by the Mesinian Evaporites as mapped at Base Salt (Fig. 9C). More precisely, it is the Lower Evaporitic Unit that forms the seal at the Base Salt with localised thickness variation, while the Upper Evaporitic Unit remains relatively isopachous across the underlying traps.

### 5.3. Pressure history reconstruction

Pressure history reconstruction for the pipe trails is based on the widely accepted view that fluid escape pipes form by hydraulic fracturing (Cartwright and Santamarina (2015) and refs therein), and follows the approach adopted by (Cartwright et al., 2021). Hydraulic fracturing is the only conduit-forming process that can viably explain high flux transmission of fluids and even mud across thick evaporite sealing sequences (Kirkham et al., 2018). In the case of the pipe trails in the study area, high fluid fluxes and probably high velocities are implied by the excavation of near surface sediments to form the pockmarks with 10s of meters of relief at the pipe outlets (Fig. 8). Similar arguments apply to those outlets composed of small mud volcanoes where individual fractures within the salt maintained aperture during active extrusion of the highly overpressured mud slurry (Kirkham et al., 2018b).



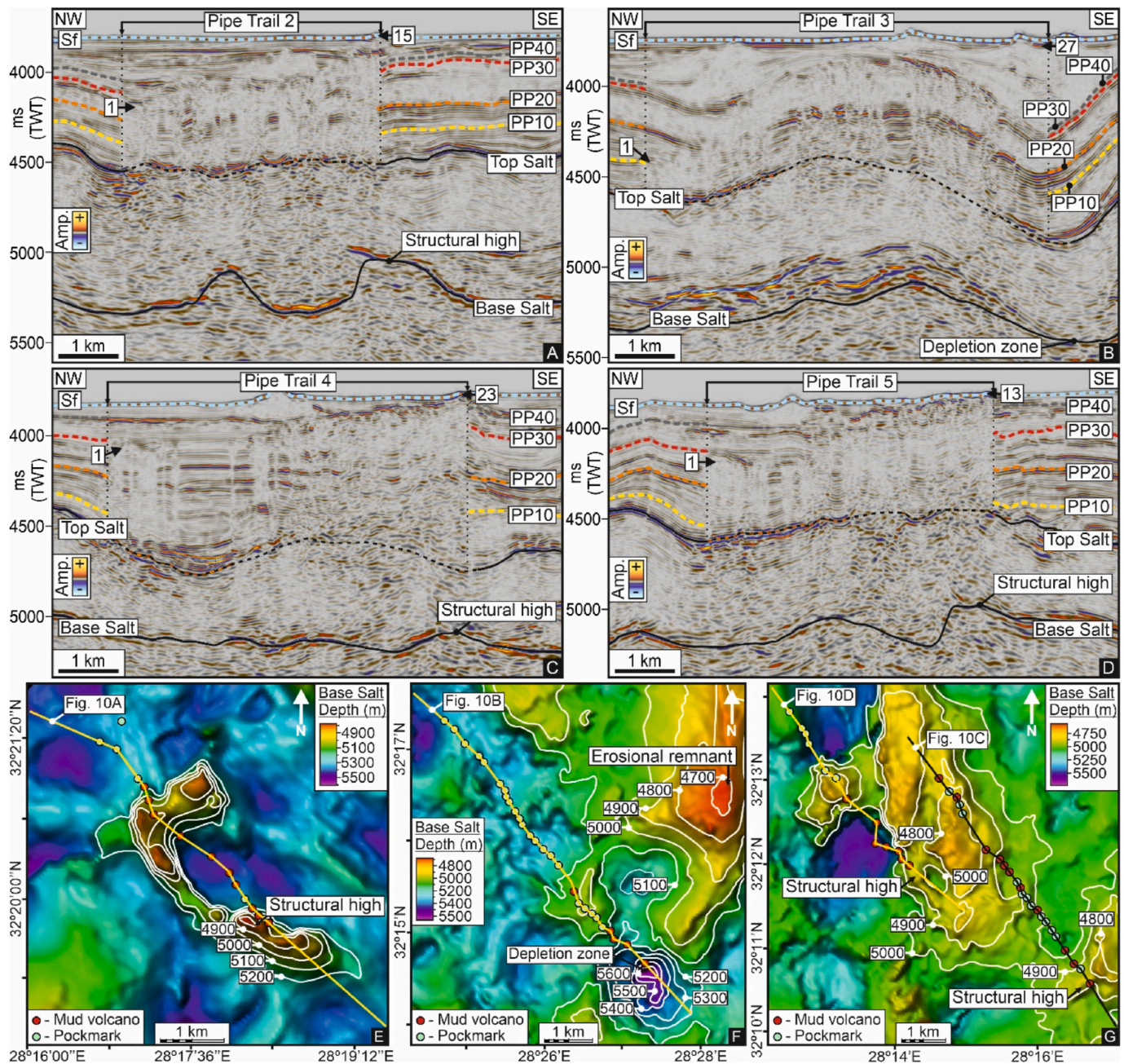


**Fig. 10.** Episodic venting in Pipe Trails (PT) 2–5, sourced from erosional stratigraphic traps at the Base Salt. **A–D:** Two-way time seismic cross-sections through PT2–PT5 (modified from Kirkham and Cartwright (2021); see Fig. 10E–G for line locations) showing the linear distribution of pipes in the pipe trails and positioning of the pipe outlets at progressively deeper horizons to the NW. The most recent outlet in each PT is positioned at the seafloor. **E–G:** Depth maps and structure contours (in meters) of the Base Salt (see Fig. 5B for locations) with the position of the mud volcano and pockmark outlets in PT2–5 overlain. The most recent pipe in PT2, 4 & 5 are positioned overlying stratigraphic traps (structural highs; see also Fig. 10A–D). The most recent pipe in PT3 is located above a depletion zone at the Base Salt that is positioned at the SW end of an erosional structural high.

Importantly, since the pipes are interpreted to root to the crest of stratigraphic traps as mapped at the Base Salt (Figs. 8A, 9 and 10), the critical fluid pressure for hydraulic fracture propagation across the >1000 m thick salt layer must have been achieved at the sediments crestal position at the Base Salt within OM2 (Figs. 9 and 10). The pressure conditions can be reconstructed straightforwardly by combining the conditions necessary for hydraulic leakage with the geometry of the leakage position. Using this approach, we reconstructed the pressure history for PT1, 2, 4 and 5, where the pre-salt structure was not modified by later mud extrusion.

The reconstructed pressure-depth plot for the largest of the

stratigraphic traps, the Kiwi High, is presented to illustrate the approach in detail (Fig. 13). Using a modest differential stress of 2 MPa and negligible tensile strength (0 MPa; alternatives are discussed in section 6.3.2), a conservative estimate of the pore fluid pressure required to initiate hydraulic failure of the base of the salt for the formation of the most recent pipe in the trail is calculated as 57.4 MPa ( $\pm 1$  MPa) (Fig. 13A). This is close to, but just smaller than the total overburden stress at this point.

Since we find no evidence of local deformation around the stratigraphic traps that formed the loci for episodic venting along the pipe trails, we can reconstruct the pressure conditions extant at the start of

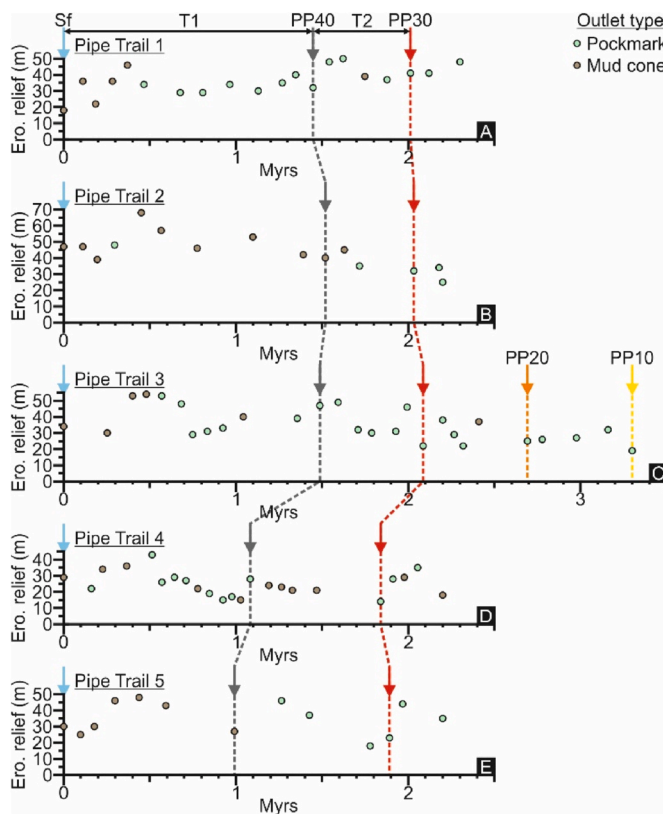
**Table 1**

Key details and statistics from Pipe Trails 1-5.

Pipe trail	Number of venting episodes	Number of venting episodes during T1	Number of venting episodes during T2	Number of pockmarks	Number of mud volcanoes	Erosional relief of outlets
1	20	4	11	14	6	19–52
2	15	2	8	10	5	26–72
3	27	5	10	21	6	20–57
4	23	4	12	12	11	15–45
5	13	3	5	6	7	19–50

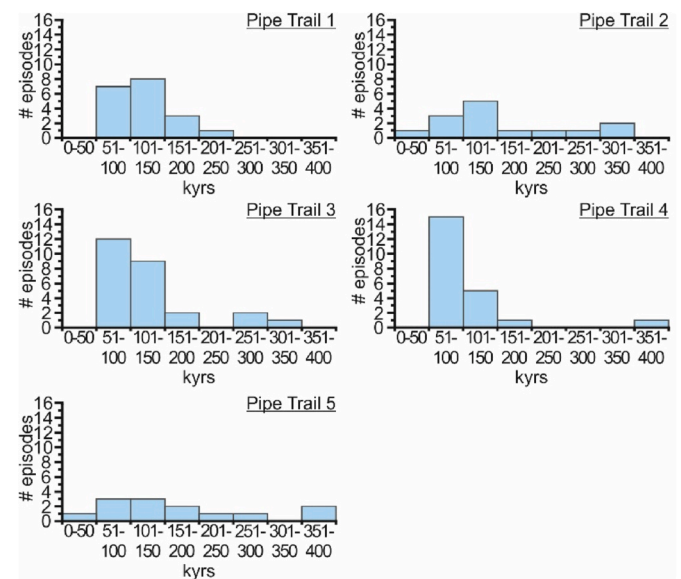
  

Pipe trail	Pipe spacing range (m)	Average pipe spacing (m)	Age of first pipe (Ma)	Pipe trail translation distance (m)	Average Post Salt translation velocity (mm/yr)	Time range between venting episodes (kyrs)	Average time between venting episodes (kyrs)
1	139–416	234	2.3	4260	1.9	73–211	121
2	149–578	317	2.2	3830	1.7	22–324	157
3	120–602	251	3.3	6330	1.9	53–313	127
4	138–944	260	2.2	5610	2.6	51–371	100
5	146–813	383	2.2	4270	1.9	77–398	183

**Fig. 11.** Timing of venting and pipe formation in Pipe Trail 1–5. The plots show the timing of venting episodes (see data methods for how timing is constrained) and the erosional relief interpreted for each outlet in PT1–5. The position of key markers horizons (seafloor (Sf) and PP10–40) that are interpreted across the pipe trails (see Figs. 9A and 10A–D) and two relative time intervals (T1 & T2) are correlated between the plots.

each pipe trail. This is straightforward: we simply remove the overburden load added during the period following the first vent in the pipe trail and plot the pressure–depth curve using the same density values for the different units, with a reduced overburden, but a constant water depth (Fig. 13B; see Section 4). For PT1 at the Kiwi High, 335 m of overburden is removed in the pressure vs depth plot (Fig. 13B). The calculated fracture pressure for the oldest pipe in the trail is therefore 50.7 MPa ( $\pm 1$  MPa) (Fig. 13B), considerably less than that required for the most recent pipe to form.

Initial and final pressure conditions for initiating hydraulic failure of the salt seal for the three other pipe trails where we could make the

**Fig. 12.** Histograms for Pipe Trails 1–5 showing the frequency of venting episodes binned in 50 kyr intervals between one venting episode and the next (see Fig. 11 for intervals).

reconstruction are presented in Table 2, and show similar histories to that described for PT1, with a general increase of a few MPa from the onset to the final pipe in each trail.

## 6. Discussion

The study area in the West Nile Deep Sea Fan contains an unusually high density of fluid flow features whose formation involves breaching of the thick Messinian salt seal. This observation alone indicates that the Pre-Salt of this area must be anomalously overpressured with respect to neighbouring parts of the basin, where such features are more sporadically developed. This highly dynamic fluid migration from the Pre Salt to the contemporaneous surface occurred as isolated singular foci for pressure venting over a protracted period following the conclusion of the Messinian Salinity Crisis to the present day, so it is reasonable to infer that the anomalous overpressure was inherited from this globally significant environmental event (Al-Balushi et al., 2016; Bertoni and Cartwright, 2015). Within this broader context of intensive pressure venting, the five pipe trails documented here stand out as exceptions in as much as they are the only ‘valves’ that opened and shut repeatedly over a prolonged period of time.

The episodic nature of the venting in these five locations prompts a



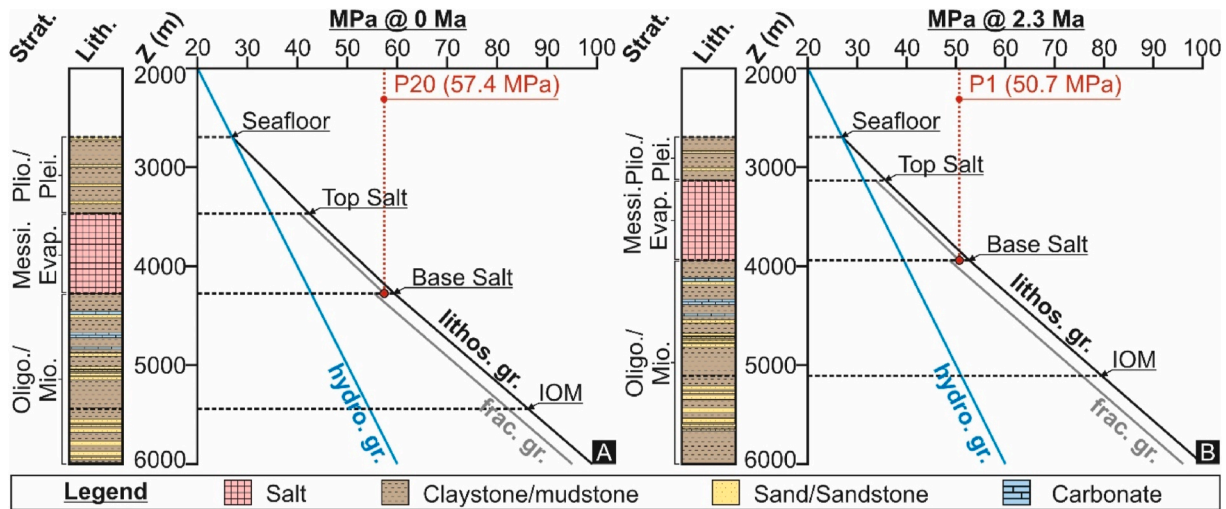


**Fig. 13.** Pressure-depth (P-z) plots for pipe formation above the Kiwi High. **A:** Proposed stratigraphic column in depth at the crest of the Kiwi High and a P-z plot for the most recent pipe (P20) in PT1 (see data methods for gradient constructions). A pressure of 57.4 MPa ( $\pm 1$  MPa) is required to initiate hydraulic fracturing at the Base Salt. **B:** A reconstructed stratigraphic column in depth and P-z plot for the first pipe (P1; 2.3 Ma) in PT1. A comparatively lesser pressure of 50.7 MPa ( $\pm 1$  MPa) is required to initiate hydraulic fracturing at the Base Salt. Gr – gradient, Lith. – lithology, Lithos. – lithostatic, Frac. – fracture, Hydro. – hydrostatic, Strat. – stratigraphy, Plio./Plei. – Pliocene/Pleistocene, Messi. Evap. – Messinian Evaporites, Oligo./Mio. – Oligocene/Miocene.

**Table 2**

Pressure requirements to initiate hydraulic failure at the Base Salt for the first and most recent pipes in PT1, 2, 4 & 5. Pressure conditions cannot be given for PT3 because the Base Salt geometry when the pipes formed has been modified by the formation of a large depletion zone (see Fig. 10B and F).

	PT1	PT2	PT3	PT4	PT5
First pipe fracture pressure (MPa)	50.7	59.4		56.1	62.6
Most recent pipe forming fracture pressure (MPa)	57.4	67.2		65.7	67.5
Pressure difference (MPa)	6.7	7.8		9.6	4.9

number of questions, namely, what is the pressure evolution within the pipe trail system, what controls the timing and pressure requirements for episodic venting, what overpressuring mechanism are responsible for the initial overpressure generation and continued pressure recharge?

### 6.1. Pressure evolution

The episodic valving of pressure exhibited by all five trails requires that the pressure conditions for hydraulic leakage must be achieved repeatedly, separated by intervals of 50–250 Ka where the pressure was

below this threshold. The episodic fluid venting expressed in the pipe trails exhibits all the characteristics of cyclical pressure valving first modelled by Roberts and Nunn (1995). They envisaged a process involving pressure increase to the threshold for hydraulic fracturing followed by fluid expulsion via the fracture network as the fractures propagate. The fluid expulsion from the overpressured compartment at depth would then result in an almost instantaneous (geologically) pressure drop leading in turn to closure of the fracture network once the pressure at the tip decreased to the fracture closure pressure, assumed to be the minimum stress (c.f. Hubbert and Willis (1957)). Once the fractures have closed, pressure increases again in the overpressured compartment.

We envisage a similar sequence of events as those modelled by Roberts and Nunn (1995) to explain the development of the episodic pipe trails in the study area (Fig. 14). Fluid pressure within OM2 is considered to have been anomalously high as a result of events linked to the Messinian Salinity Crisis, culminating in the earliest Pliocene reflooding of the Mediterranean (Garcia-Castellanos et al., 2009). The pressure within the trap must have continued to build steadily upwards through the early to mid Pliocene to the point where an initial pipe formed at the crest of the stratigraphic trap (Pf, fracture pressure; Fig. 14A). The initial fracture network for the pipe propagated upward

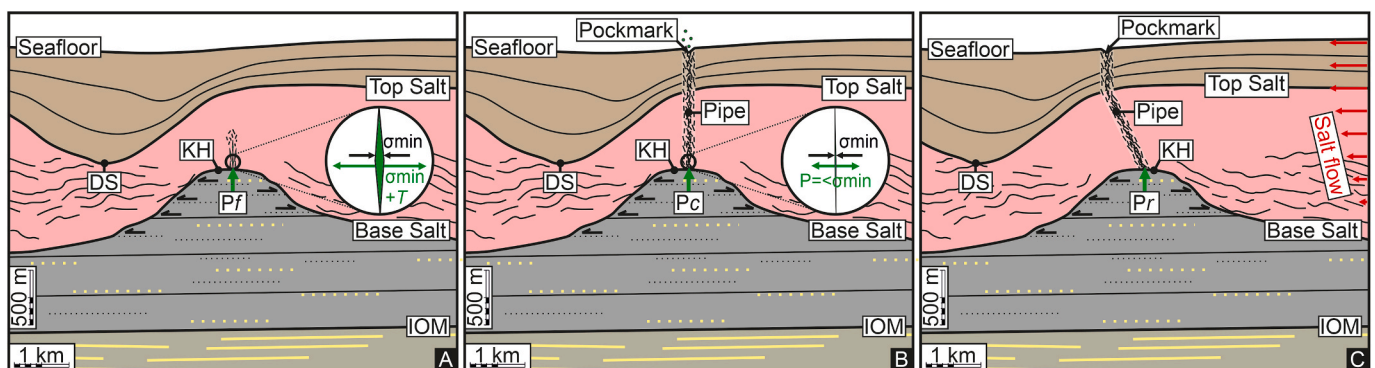


**Fig. 14.** Model for episodicity in hydraulic fracture pipe formation. **A:** Pressure at the crest of the Kiwi High (KH) is at least equal to the fracture pressure ( $P_f = \sigma_{min} + T$ ), initiating hydraulic failure at the Base Salt. DS – dissolution structure. **B:** A pressure drop, during pressure valving, at the crest of the trap and in the fractures decreases to the fracture closure pressure ( $P_c$ ;  $P_c < \sigma_{min}$ ). The fractures close and cease acting as conduits. **C:** The pipes fracture network is displaced basinward by the flowing salt, rebuilding the integrity of the seal overlying the trap. Pressure is recharged in the trap ( $P_r$ ) for the next venting episode in the cycle.

through the entire salt and claystone overburden. Pressure recovery at the crest of the stratigraphic trap must have been rapid enough to continually provide the volume of fluids and pressure required to fill the porosity of the fractures and continue to drive the propagation of new fractures to the seafloor. This requires the hydraulic diffusivity in the source region to be sufficient to transmit the fluid volume and pressure needed for pressure recovery. The rapid (geologically) venting of fluids decreased the pressure within the stratigraphic trap. Fluid migration through the fracture network ended when the pressure in the stratigraphic trap decreased to the point where the pressure in the connected fluid column at the top of the pipe decreased beneath the fracture closure pressure ( $P_c$ ; equal to the minimum stress; Fig. 14B). Sediments then buried the outlet for the pipe once venting ended and the north-westerly flowing salt displaced the pipe from above the crestal locus, rebuilding seal integrity overlying the trap. The pressure in the stratigraphic trap would then recharge by whatever pressure building mechanisms were extant immediately prior to the initial pipe formation combined with the type of local recharge mechanism envisaged by Roberts and Nunn (1995) (Pr, pressure recharge; Fig. 14C) (see also Luo and Vasseur (1995)). Pressure recharge in the stratigraphic trap back to the fracture pressure is marked by the formation of the next individual fluid escape pipe and outlet in the pipe trail.

This cyclical process is best expressed by some kind of sawtooth pressure evolution (Fig. 15A) analogous to oscillations in igneous volcanic activity (Kanno and Ichihara, 2018), geyser eruptions (Hurwitz and Manga, 2017) and mud volcano eruptions (Deville and Guerlais, 2009). A reconstruction of one potential sawtooth pressure evolution for PT1 is presented in Fig. 15A. The pressure-time plot utilises the pressure depth plots for PT1 (Fig. 13) and timing for pipe formation (Fig. 11A) to reconstruct the pressure evolution in the trap (c.f. Cartwright et al. (2021)).

## 6.2. Comparison with previously reported pipe trails

The pipe trails described in this study share some similarities to those reported previously from the North Levant Basin (e.g. Fig. 2) by Cartwright et al. (2021) and Oppo et al. (2021b). Both geographical groups of pipe trails involve hydraulic fracture propagation through thick salt layers, that would typically be regarded as highly efficient seals (Fig. 16). In addition, the typical range of time intervals between venting episodes is similar in both areas, namely in the 50-250Ka range. However, there are several fundamental differences. The pipe trails in the North Levant Basin root to the crest of anticlinal structural traps from the top of a putative Oligo-Miocene sandstone reservoir in the pre-salt that is juxtaposed with an immediate top seal comprising Miocene claystones (Fig. 16A). By contrast, the pipe trails in the West Nile Deep Sea Fan root to the crest of erosional stratigraphic traps that confine a parallel stratified and dominantly Late Miocene succession that is also the overpressured source of hundreds of mud volcanoes in the region, with an immediate top seal of Messinian Evaporites (Fig. 16B). Important contrasts in the overpressure mechanisms for the pipe trails in these two regions are discussed in section 6.4.

Does the trap configuration have any influence on the formation of episodic venting features? Reverse faults bound the lateral margins of many of the pre-salt folds in the North Levant Basin (Fig. 16A) (Cartwright et al., 2018, 2021) and it has been proposed that normal faults imaged within the resolution of seismic reflection data that cross-cut these folds could act as barriers or baffles to lateral fluid movement, resulting in partial or fully compartmentalised reservoirs (Oppo et al., 2021b). In the West Nile Deep Sea Fan, enclosure of the parallel stratified OM2 within the erosional stratigraphic traps and juxtaposition with the Messinian Evaporites also forms a potentially effective pressure compartment (Fig. 16B). It is, therefore, reasonable to postulate that compartmentalisation or formation of a pressure compartment may be an important factor to facilitate geologically rapid pressure recharge within a pressure cell (c.f. Moss and Cartwright (2010b)) for episodic

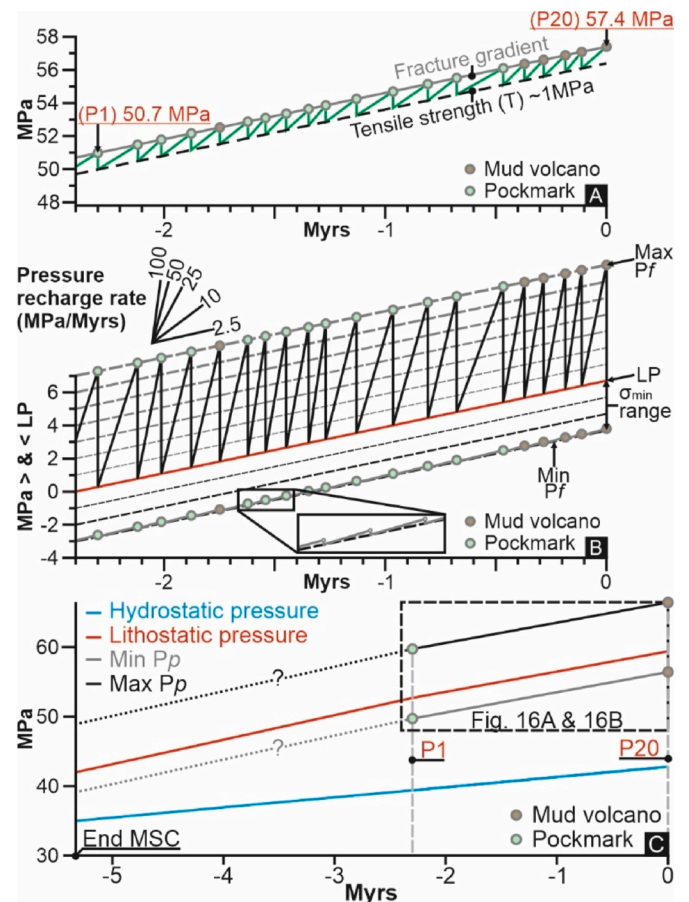


Fig. 15. Pressure-time (P-t) plots for Pipe Trail 1 (PT1) and the Kiwi High. A: P-t plot showing a potential sawtooth pressure evolution since the onset of PT1 following the methodology in Cartwright et al. (2021), reconstructed from the pressure depth plots in Fig. 13 and interpreted pipe timings in Fig. 11A. P1 - pipe 1; P20 - pipe 20. B: A P-t plot showing the minimum and maximum pressure conditions, pressure recharge rates and pressure evolution for PT1. A minimum fracture gradient (Min Pf) of 2.9 MPa below the lithostatic pressure (LP) is given based on a differential stress of 3 MPa and tensile strength of 0.1 MPa. A maximum fracture gradient of 7 MPa above the LP is given, with an isotropic state of stress and tensile strength of 7 MPa. C: Pressure evolution at the crest of the Kiwi High since the Messinian Salinity Crisis (MSC). Pp - pore fluid pressure.

venting.

Cartwright et al. (2021) considered the fracture pressure ( $P_f > \sigma_{min} + T$ ;  $\sigma_{min}$  - minimum stress,  $T$  - tensile strength) at the top seal as a minimum requirement to initiate hydraulic fracturing and pipe formation, with higher pressures possible. Cartwright et al. (2021) reconstructed the pressure evolution in the trap leading up to and during the period of venting and argued for a similar sawtooth pressure evolution to that inferred in our study in the Herodotus Basin. However, neither Cartwright et al. (2021) nor Oppo et al. (2021) considered in any detail the uncertainties in dating of event, nor in the fracture pressure hence it is hard to evaluate their suggestions for causal mechanisms of initial and subsequent venting against the range of possible overpressuring mechanisms.

## 6.3. Uncertainties in dating and fracture conditions

### 6.3.1. Dating the expulsion events

The main source of error in the analysis of the timing of the episodic venting history is the assumption of a constant salt flow velocity through the venting period. This assumption allows us to use the outlet distance



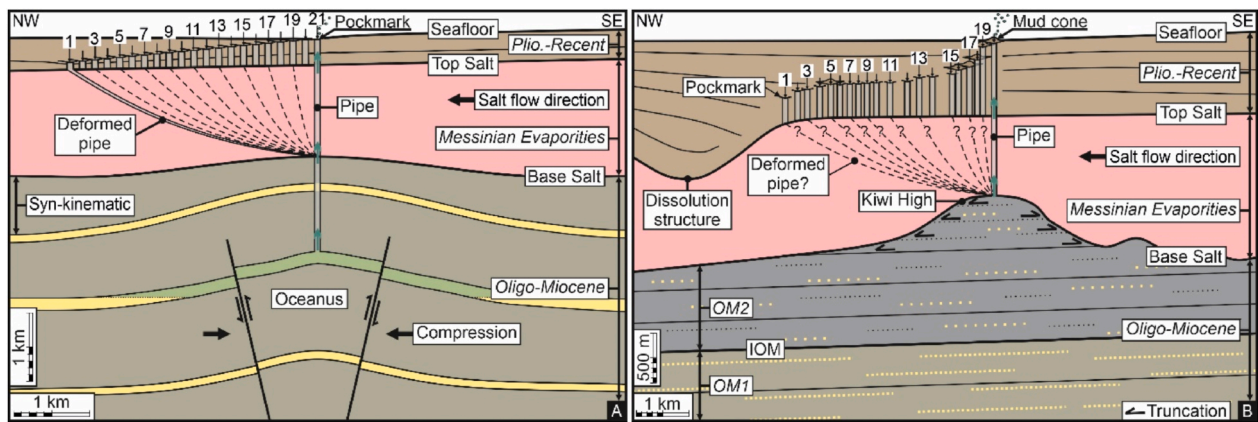


**Fig. 16.** Comparison between pipe trails in the West Nile Deep Sea Fan and the North Levant Basin. **A:** A schematic cross-section through the Oceanus pipe trail in the North Levant Basin (modified from Cartwright et al. (2021)). The pipe trail roots to the crest of a folded sandstone reservoir in the Oligo-Miocene, with a claystone top seal. Reverse faults bound the NW and SE margins of the fold. **B:** A schematic cross-section through PT1 in the West Nile Deep Sea Fan. The pipe trail roots to the crest of an erosional stratigraphic trap. The Late Miocene stratigraphy within the trap is parallel stratified and dominantly claystone, with a salt top seal. The pipes are numbered in the order of their formation. The geometry of the deformed pipes within the Messinian Evaporites is inferred from the expected Couette flow regime within the salt in this region (Kirkham and Cartwright, 2021). OM – Oligo-Miocene, IOM – Intra-Oligo-Miocene.

to date individual events. Successive outlets are always at younger horizons, so the individual events always young systematically towards the expulsion locus (Fig. 2) and any deviation from this average velocity cannot violate this condition. In practice, this means we cannot invoke rapid accelerations or decelerations in salt flow. Since the driver for salt flow is regional tilting of the basin (Kirkham and Cartwright, 2021; Zucker et al., 2020), such rapid fluctuations are unlikely.

It is conceivable, however, that the salt flow velocity has undergone periods of gradual acceleration or deceleration. Kirkham and Cartwright (2021) interpreted a 10–20% increase in translation velocity between the initial formation of the dissolution structure that formed at c. 4 Ma and the onset of the pipe trail in PT1 some 2 million years later. While the potential error due to such gradual changes is unlikely to have a substantial impact on the inter-event durations, the cumulative error through the full venting history of each trail may be significant and potentially explain the observed mismatch for PT4 and PT5 (Fig. 11D and E).

### 6.3.2. Fracture conditions

The minimum stress value within the salt and its tensile strength are the two main sources of uncertainty in the estimation of the pressure conditions necessary to initiate propagation of a hydraulic fracture network through the salt. These derive directly from the failure condition,  $P_f > \sigma_{\min} + T$  (Price and Cosgrove, 1990). In studies dealing with borehole stability whilst drilling through salt, it is common practice to assume that the minimum and maximum stress are equal ( $\sigma_{\min} = \sigma_{\max}$ ) or that the state of stress is isotropic because the salt behaves as a viscous fluid on geological time scales (Fredrich et al., 2003; Dusseault et al., 2004). However, studies on salt microstructure have been used to argue that there is a probable range of differential stress within flowing salt layers of 1–3 MPa (Schoenherr et al., 2007; Weijermars and Jackson, 2014). This difference in views on the state of stress within thick salt layers should probably be regarded as the uncertainty in the value of  $\sigma_{\min}$ .

The strength of salt is dependent on the material composition of the salt type, water content, stress conditions and temperature of the salt in situ (Sriapai et al., 2012; Willson and Fredrich, 2005). Estimates of the tensile strength of salt sequences of 1–3 MPa have been made from analyses of extended leak-off tests (Bérest et al., 2015). A modest value 1.65 MPa has been cited for the tensile strength of the salt in the Gulf of Mexico from direct tension testing (Willson and Fredrich, 2005). A crude estimate of tensile strength can also be made from practical experience of safe drilling windows through salt. Mud weights at the shoe of a well

that is overbalanced by a maximum of 5 MPa is advised when drilling through intact salt, although <3 MPa is preferred, to prevent creep whilst also not fracturing the rock (Dusseault et al., 2004). Willson and Fredrich (2005) note that an upper limit for a formation integrity test is set at overburden plus 4 MPa. This would imply a tensile strength of 5–7 MPa assuming the range of differential stress values taken from Schoenherr et al. (2007) and Weijermars and Jackson (2014). Finally, laboratory measurements of the tensile strength of virtually pure halite at varying temperatures show a linear decrease in salt strength as temperature increases, from ~4.8 MPa to 7.3 MPa (Sriapai et al., 2012). Taking these different types of estimate together, it is evident that the tensile strength of salt could range from almost zero to about 7 MPa.

What is clear from this preceding discussion is that despite any uncertainty in the fracture pressure, the pressure conditions required for each venting episode are close to or in excess of the lithostatic pressure (the vertical overburden stress). From the sawtooth history plots shown in Fig. 15B, it is evident that the time between venting episodes is a function of fracture pressure ( $P_f$ ), fracture closure pressure ( $P_c$ ) and the pressure recharge rate ( $Pr = dp/dt$ ;  $dp$  = change in pressure,  $dt$  = change in time) to again reach the  $P_f$ . The tensile strength is thus the key variable in defining the shape of the sawtooth, with a large tensile strength requiring both a greater pressure drop to reach  $P_c$  and subsequently a greater amount of pressure recharge to reach  $P_f$  again (Fig. 15B).

### 6.4. Overpressure generation and pressure recharge

The pipe trails in the study require the generation of pore fluid pressures close to or even above the lithostatic pressure in the Pre Salt soon after deposition of the Messinian Evaporites. We now discuss the mechanisms that are responsible for generating this pressure and reliably recharging pressure in the West Nile Deep Sea Fan for this episodic venting.

#### 6.4.1. Overpressure generation during the Messinian Salinity Crisis

The Eastern Mediterranean underwent several major phases of unloading and loading during the Messinian Salinity Crisis that must have modified the pore pressure in the Pre Salt (Bertoni and Cartwright, 2015; Al-Balushi et al., 2016). These include (1) an early stage draw-down that has been interpreted to have triggered gas venting at the Base Salt palaeo seafloor (Bertoni et al., 2013); (2) rapid deposition of the regionally sealing Messinian Evaporites, leading to undercompaction of the Pre Salt and high pore-water retention (Kirkham et al., 2017, 2018a); (3) a late Messinian drawdown that led to a phase of thermally

driven dissolution at the top of the salt (Kirkham et al., 2020a) (4) rapid seawater loading during the Zanclean flood (Garcia-Castellanos et al., 2009).

The extrusion of giant mud volcanoes/mud canopies directly on top of the salt (Kirkham et al., 2018a, 2020b) and the continued mud volcanism and fluid venting through the salt immediately following the Messinian Salinity Crisis is a strong indication that overpressure in the upper Miocene in this study area was primed by the loading and unloading events during the Messinian salinity Crisis and has remained highly overpressured over at least the last ~5.33 Myrs and possibly prior to this (Fig. 15C). It is reasonable to expect that the stratigraphically trapped compartments of OM2 in the Pre Salt were initially overpressured to near the fracture pressure due to undercompaction (Fig. 15C). Vertical and lateral sealing of the trap by the Messinian Evaporites is likely to have impeded pressure transfer out of the trap (Muggeridge et al., 2004) and resulted in the retention of high pore pressure since the Messinian Salinity Crisis.

#### 6.4.2. Pressure recharge mechanisms

Whilst the overpressure required for a single venting episode can be substantially attributed to the events linked to the Messinian Salinity Crisis, how is pressure in the Pre Salt traps in the West Nile Deep Sea Fan recharged for multi-episode venting? We can exclude several common mechanisms because of the geological context:

- (1) Tectonic compression: interpreted by Cartwright et al. (2018) as a key mechanism for the pipe trail in the North Levant Basin (Fig. 16A). However, there is no evidence of contractional structures in the Pre Salt in the West Nile Deep Sea Fan, nor do the pipes root to the crest of contractional folds.
- (2) Pressure Transfer from the deep basin: proposed by Oppo et al. (2021b) as another key mechanism for the pipe trail in the North Levant Basin. However, the stratigraphic traps in the West Nile Deep Sea Fan consist of low permeability claystones of the shallow dipping OM2 that are confined by truncation to within the erosional margins of the trap and sealed laterally and above by the thick salt layer.
- (3) Sea level change: the magnitude of pressure excursions due to eustatic changes in sea level are too small.
- (4) Diagenesis: cannot be completely excluded, but there is no evidence from direct samples taken from the mud volcanoes in the study area for smectite having converted to illite in OM2 (c.f. Giresse et al. (2010)).
- (5) Buoyancy pressure: no evidence for any reservoirs hosting sufficiently thick hydrocarbon columns trapped beneath the salt. However, thermogenic and biogenic methane has been sampled from mud volcanoes in the study area (Prinzhofer and Deville, 2013), suggesting that hydrocarbon generation rather than buoyancy could be a viable mechanism.

By elimination therefore, we are left with three possible overpressure generating mechanisms to explain the recharge between venting episodes. A single overpressuring mechanism is unlikely to be responsible for the pressure recharge, but rather a combination of:

- (1) Disequilibrium compaction – An important overpressuring mechanism during the Messinian Salinity Crisis due to rapid loading of the salt; but only a minor contributor during the Pliocene-Recent (6–10 MPa  $\pm$  1 MPa) due to low sedimentation rates in a deepwater (3 km water depth) setting. Disequilibrium compaction cannot increase pore fluid pressure above the lithostatic pressure. Furthermore, whilst gradual loading will have increased pore fluid pressure in the stratigraphic traps as the salt seal impedes dewatering, the lithostatic pressure will also increase making repeatedly reaching the fracture criteria by disequilibrium compaction alone unlikely.

- (2) Hydrocarbon generation – Modelling of the thermal gradient in the Eastern Mediterranean (Al-Balushi et al., 2016) and brine temperatures of up to 57 °C recorded from within the Chephren mud volcano in the study area (Dupré et al., 2014) provide an insight into the temperature of the fluids and mud remobilized from OM2. OM2 is thermogenically immature and so the thermogenic gas sampled from the mud volcanoes in this study area (Prinzhofer and Deville, 2013) must have been generated at greater depths in the Pre Salt than the pipe trails root to. OM2 is, however, within the biogenic window and so biogenic gas generation within the appropriate temperature window in the stratigraphically trapped compartments could be a significant source of overpressure. This mechanism has been invoked as a major source of overpressure and linked to the formation of gas venting features elsewhere, but is at present poorly quantified (Tingay et al., 2013; Luo and Vasseur, 1996; Mandl and Harkness, 1987; Osborne and Swarbrick, 1997).
- (3) Pressure transfer – Regional pressure transfer laterally along sandstone beds (c.f. Javanshir et al. (2015) and or upward along faults (c.f. Grauls and Baleix (1994)) is unlikely here due to the parallel stratification of the Oligo-Miocene (Figs. 4 and 6), the lateral confinement of the stratigraphic traps (Figs. 8 and 9) and the absence of seismically visible deep rooted faults within the traps. However, evidence for lateral transfer of near-lithostatic overpressure along shallow and low permeability sediments has been increasingly observed (Oppo et al., 2021a). Local pressure re-equilibration in the sense advocated by Roberts and Nunn (1995) and Luo and Vasseur (1995) within the dominantly claystone lithofacies of the OM2 could play an important role. These authors suggested that leakage during a venting episode leads to local de-pressuring beneath the fracture closure pressure ( $P_c$ ), and after the seal is re-established, the pressure would recharge by equilibration with the surrounding medium whose elevated pressure state (at least  $> P_c$ ) was not affected by the leakage. Local pressure transfer will wholly or partially recharge pressure following venting episodes if the volume and hydraulic diffusivity of the surrounding medium permits. However, this mechanism can only eventually recharge the local pressure to that of the surrounding medium. Additional pressure contributions will be required for further venting episodes if the pressure of the surrounding medium is less than the fracture criterion.

An intriguing observation is the hundreds of other pipes that emanate from stratigraphic traps at the Base Salt, but result in only a single venting episode in stark contrast to the episodic pipe trails with their history of repetitive venting. This implies that it has not been possible to recharge pressure within their source to the fracture criterion. The reason for this is cryptic, however, the observation that the stratigraphic traps for the pipe trails have significantly greater structural relief than those for the single episode pipes (see Sections 5.2.1 and 5.2.2.2) indicates that trap volume and hydraulic diffusivity may be an important factor. A speculative explanation is that after pressure is diminished locally beneath the structural crest within one of these comparatively small stratigraphic traps following a venting episode there is an insufficient volume of still highly pressured sediments in the trap to recharge the de-pressured cell.

#### 6.4.3. Wider implications

To date, merely a handful of papers have described direct seismic evidence for episodic venting in sedimentary basins (Andresen and Huuse, 2011; Cartwright et al., 2021; Oppo et al., 2021b; Roberts and Nunn, 1995). An intriguing aspect of the pipe trails here in the western Nile when compared to the pipe trails described in the North Levant Basin (Cartwright et al., 2018; Kirkham et al., 2019; Oppo et al., 2021b) is that the process of episodic salt seal failure and pressure recharge was achieved over comparable periods of time and intervals between venting



episodes, but by a seemingly very different set of mechanisms. The pipe trails discussed here demonstrate that these episodic venting phenomena are not uniquely restricted to a single basinal setting and that they may be expected to occur far more widely in other basins with high quality seals. Furthermore, there is no single mechanism that is responsible for the pressure recharge that drives episodic venting, but several are possible and act together, further broadening the potential sedimentary basin setting in which they may be found.

A unique aspect of the pipe trails in the Eastern Mediterranean is that the lateral offset of pipes and outlets away from their genetically connected root by the flowing salt has made the interpretation of each discrete venting episode relatively straightforward in 3D seismic reflection data. Similar episodic venting phenomena and pressure recharge are almost certain to be present in other basins globally, but may have been overlooked due to the challenges in identifying individual outlets within the vertically disturbed zone of fluid venting (Andresen and Huuse, 2011). The common elements from the small handful of examples that exist are a source region that is highly overpressured to near or supra-lithostatic pressure, trap configurations that are overlain by an effective seal such as salt and are partially or fully compartmentalised, and pressure recharge that is efficient enough to reach the fracture criteria more than once. It is conceivable that regions such as offshore Brazil and Gabon where there are large scale base salt structures may contain similar episodic venting phenomena. Extreme caution should be taken during the planning and drilling of such structures as the Kiwi High due to the hazardously high overpressure therein.

## 7. Conclusions

A total of 382 individual fluid escape pipes and 5 linear fluid escape pipe trails are distributed throughout the study area in the West Nile Deep Sea Fan. The pipes and pipe trails root to the crest of erosional stratigraphic traps at the Base Salt, transect >1 km of Messinian Evaporite and terminate upwards at outlets that are either pockmarks or mud cones in the Pliocene to Recent. The pipe trails present evidence of rarely documented multi-episode venting and failure of a thick sealing salt layer. These pipes are formed by hydraulic fracturing of the thick salt and claystone seal and their genesis requires extreme overpressure and efficient pressure recharge in the pre-salt traps.

The pressure in the pre-salt traps necessary to form the pipes must have been a magnitude equal to at least the hydraulic failure criteria for the salt seal ( $P_{fmin} = \sigma_{min} + T$ ). The pressure requirements are near to or potentially above the lithostatic pressure depending on the different stress ( $\sigma_{min}$ ) and tensile strength ( $T$ ) of the salt. The episodic nature of the pipe trails implies that the extreme high pressures that are required for hydraulic failure of the salt seal have been repeatedly achieved every ~50–150 kyrs. The pressure evolution in the pre-salt traps over the lifetime of the episodic pipe trails is best expressed by a sawtooth pressure evolution.

Mud volcanoes extruded in the lowermost Pliocene that are sourced from the same pre-salt interval in the study area as the pipes suggest that the Pre Salt was undercompacted and already highly overpressured following the Messinian. Pressure recharge required for episodic venting could be achieved in the West Nile Deep Sea Fan by a combination of biogenic gas generation and pressure transfer within the pre-salt traps, with some minor contribution from disequilibrium compaction.

Prior to this study, similar pipe trails had only been interpreted in the North Levant Basin. The pipe trails in the West Nile Deep Sea Fan widen the recognition of these episodic venting phenomena beyond a single basin and suggests that their genesis can be achieved by contrasting trap, reservoir and seal configurations and pressure recharge mechanisms. Salt has often been considered as a 'perfect' seal in hydrocarbon systems, however, the pipe trails demonstrate that it is possible to repeatedly breach a thick salt layer over a period of a few million years. This has significant implications for prospect de-risking during pre-salt hydrocarbon exploration, as well as pre-salt CO<sub>2</sub> storage and hydrogen storage

in salt caverns. These episodic venting features show that extreme overpressure can be maintained within this type of trap and seal configuration and presents a significant hazard while drilling. Similar venting features should be present in other basins globally with analogous trap and seal configurations and suitably efficient pressure recharge mechanism. We expect that future works will broaden the global recognition of these episodic venting phenomena and further our understanding of the type of basin settings, overpressuring mechanisms and palaeo and recent overpressure at depth.

## Data availability statement

The data used for this research is confidential industry seismic reflection data and cannot be shared.

## Declaration of competing interest

The authors declare that they have no known competing financial interests or personal relationships that could have appeared to influence the work reported in this paper.

## Acknowledgments

We would like to thank the Editor Davide Oppo and the two anonymous reviewers for their constructive comments that led to an improved manuscript. We are grateful to Equinor for provision of the 3D seismic data and Schlumberger for provision of the seismic interpretation software. We thank the entire Seismic Lab team in Oxford and Claudia Bertoni, Richard Katz, Chris MacMinn and Martino Foschi for the many helpful discussions.

## References

- Aal, A.A., El Barkooky, A., Gerrits, M., Meyer, H., Schwander, M., Zaki, H., 2000. Tectonic evolution of the eastern Mediterranean basin and its significance for hydrocarbon prospectivity in the ultra-deepwater of the Nile delta. *Lead. Edge* 19, 1086–1102. <https://doi.org/10.1190/1.1438485>.
- Al-Balushi, A.N., Neumaier, M., Fraser, A.J., Jackson, C.A., 2016. The impact of the Messinian salinity crisis on the petroleum system of the Eastern Mediterranean: a critical assessment using 2D petroleum system modelling. *Petrol. Geosci.* 22, 357–379. <https://doi.org/10.1144/petgeo2016-054>.
- Allen, H., Jackson, C.A.-L., Fraser, A.J., 2016. Gravity-driven deformation of a youthful saline giant: the interplay between gliding and spreading in the Messinian basins of the Eastern Mediterranean. *Petrol. Geosci.* 22, 340–356. <https://doi.org/10.1144/petgeo2016-034>.
- Anderson, J., Cartwright, J., Drysdall, S., Vivian, N., 2000. Controls on turbidite sand deposition during gravity-driven extension of a passive margin: examples from Miocene sediments in Block 4, Angola. *Mar. Petrol. Geol.* 17, 1165–1203. [https://doi.org/10.1016/S0264-8172\(00\)00059-3](https://doi.org/10.1016/S0264-8172(00)00059-3).
- Andresen, K.J., Huuse, M., 2011. 'Bulls-eye' pockmarks and polygonal faulting in the Lower Congo Basin: relative timing and implications for fluid expulsion during shallow burial. *Mar. Geol.* 279, 111–127. <https://doi.org/10.1016/j.margeo.2010.10.016>.
- Baer, S., Lie, Ø., Almorshedy, A., 2016. New opportunities offshore west Egypt. *GEO ExPro Magazine* 13, 42–45.
- Barber, P.M., 1981. Messinian subaerial erosion of the proto-Nile Delta. *Mar. Geol.* 44, 253–272. [https://doi.org/10.1016/0025-3227\(81\)90053-0](https://doi.org/10.1016/0025-3227(81)90053-0).
- Bérest, P., Brouard, B., Fabien, F., Hévin, G., Karimi-Jafari, M., 2015. Maximum pressure in gas storage caverns. In: *Proceedings of the Solution Mining Research Institute Spring Technical Conference*. Solution Mining Research Institute (SMRI), Rochester, New York, USA.
- Bertoni, C., Cartwright, J., 2015. Messinian evaporites and fluid flow. *Mar. Petrol. Geol.* 66, 165–176. <https://doi.org/10.1016/j.margeo.2015.02.003>.
- Bertoni, C., Cartwright, J., Hermanrud, C., 2013. Evidence for large-scale methane venting due to rapid drawdown of sea level during the Messinian Salinity Crisis. *Geology* 41, 371–374. <https://doi.org/10.1130/G33987.1>.
- Bertoni, C., Cartwright, J.A., 2006. Controls on the basinwide architecture of late Miocene (Messinian) evaporites on the Levant margin (eastern Mediterranean). *Sediment. Geol.* 188, 93–114. <https://doi.org/10.1016/j.sedgeo.2006.03.019>.
- Brown, A.R., 2004. Interpretation of three-dimensional seismic data. In: *AAPG Memoir*, vol. 42. SEG investigations in geophysics, pp. 31–60. <https://doi.org/10.1190/1.9781560802884.ch2.9>.
- Cartwright, J., Huuse, M., Aplin, A., 2007. Seal bypass systems. *AAPG Bull.* 91, 1141–1166. <https://doi.org/10.1306/04090705181>.

- Cartwright, J., Kirkham, C., Bertoni, C., Hodgson, N., Rodriguez, K., 2018. Direct calibration of salt sheet kinematics during gravity-driven deformation. *Geology* 46, 623–626. <https://doi.org/10.1130/G40219.1>.
- Cartwright, J., Kirkham, C., Foschi, M., Hodgson, N., Rodriguez, K., James, D., 2021. Quantitative reconstruction of pore pressure history in sedimentary basins using fluid escape pipes. *Geology*. <https://doi.org/10.1130/G48406.1>.
- Cartwright, J., Santamarina, C., 2015. Seismic characteristics of fluid escape pipes in sedimentary basins: implications for pipe genesis. *Mar. Petrol. Geol.* 65, 126–140. <https://doi.org/10.1016/j.marpetgeo.2015.03.023>.
- Cozzi, A., Cascone, A., Bertelli, L., Bertello, F., Brandolese, S., Minervini, M., Ronchi, P., Ruspi, R., Harby, H., 2018. Zohr Giant Gas Discovery: A Paradigm Shift in Nile Delta and East Mediterranean Exploration. *Search and Discovery*, p. 20414.
- Deville, E., Guerlais, S.-H., 2009. Cyclic activity of mud volcanoes: evidences from Trinidad (SE Caribbean). *Mar. Petrol. Geol.* 26, 1681–1691. <https://doi.org/10.1016/j.marpetgeo.2009.03.002>.
- Deville, E., Guerlais, S.H., Lallemand, S., Schneider, F., 2010. Fluid dynamics and subsurface sediment mobilization processes: an overview from Southeast Caribbean. *Basin Res.* 22, 361–379. <https://doi.org/10.1111/j.1365-2117.2010.00474.x>.
- Dolson, J., 2020. The petroleum geology of Egypt and history of exploration. In: Hamimi, Z., El-Barkooky, A., Martínez Frías, J., Fritz, H., Abd El-Rahman, Y. (Eds.), *The Geology of Egypt. Regional Geology Reviews. The Geology of Egypt*. Springer.
- Dolson, J., Boucher, P., Siok, J., Heppard, P., 2005. Key challenges to realizing full potential in an emerging giant gas province: Nile Delta/Mediterranean offshore, deep water, Egypt. *Geological Society, London, Petroleum Geology Conference series* 6, 607–624. <https://doi.org/10.1144/0060607>.
- Dolson, J.C., Atta, M., Blanchard, D., Sehim, A., Villinski, J., Loutit, T., Romine, K., 2014. Egypt's Future Petroleum Resources: a Revised Look into the 21st Century. AAPG Special Volumes, Memoir, vol. 106. *Petroleum Systems of the Tethyan Region*, pp. 143–178.
- Downey, M., 1984. Evaluating seals for hydrocarbon accumulations. AAPG bulletin 68 (11), 1752–1763. <https://doi.org/10.1306/AD461994-16F7-11D7-8645000102C1865D>.
- Druckman, Y., Buchbinder, B., Martinotti, G.M., Tov, R., Aharon, P., 1995. The buried Afq Canyon (eastern Mediterranean, Israel): a case study of a Tertiary submarine canyon exposed in Late Messinian times. *Mar. Geol.* 123, 167–185. [https://doi.org/10.1016/0025-3227\(94\)00127-7](https://doi.org/10.1016/0025-3227(94)00127-7).
- Ducassou, E., 2006. Évolution du système turbiditique profond du Nil au cours du Quaternaire récent. *Atelier national de reproduction des thèses*.
- Dupré, S., Mascle, J., Foucher, J.-P., Harmegnies, F., Woodside, J., Pierre, C., 2014. Warm brine lakes in craters of active mud volcanoes, Menes caldera off NW Egypt: evidence for deep-rooted thermogenic processes. *Geo Mar. Lett.* 34, 153–168. <https://doi.org/10.1007/s00367-014-0367-1>.
- Dupré, S., Woodside, J., Klauke, I., Mascle, J., Foucher, J.-P., 2010. Widespread active seepage activity on the Nile Deep Sea Fan (offshore Egypt) revealed by high-definition geophysical imagery. *Mar. Geol.* 275, 1–19. <https://doi.org/10.1016/j.margeo.2010.04.003>.
- Dusseault, M.B., Maury, V., Sanfilippo, F., Santarelli, F.J., 2004. Drilling through salt: constitutive behavior and drilling strategies. In: *Gulf Rocks 2004, the 6th North America Rock Mechanics Symposium (NARMS)*. OnePetro.
- Evans, R.J., Davies, R.J., Stewart, S.A., 2007. Internal structure and eruptive history of a kilometre-scale mud volcano system, South Caspian Sea. *Basin Res.* 19, 153–163. <https://doi.org/10.1111/j.1365-2117.2007.00315.x>.
- Evans, S.L., Jackson, C.A.L., Oppo, D., 2021. Taking the pulse of salt-detached gravity gliding in the eastern Mediterranean. *Tectonics* 40, e2020TC006476. <https://doi.org/10.1029/2020TC006476>.
- Feng, Y.E., Steinberg, J., Reshef, M., 2017. Intra-salt deformation: implications for the evolution of the Messinian evaporites in the Levant Basin, eastern Mediterranean. *Mar. Petrol. Geol.* 88, 251–267. <https://doi.org/10.1016/j.marpetgeo.2017.08.027>.
- Fredrich, J.T., Coblenz, D., Fossum, A.F., Thorne, B.J., 2003. Stress perturbations adjacent to salt bodies in the deepwater Gulf of Mexico. In: *SPE Annual Technical Conference and Exhibition*. OnePetro.
- García-Castellanos, D., Estrada, F., Jiménez-Munt, I., Gorini, C., Fernández, M., Vergés, J., De Vicente, R., 2009. Catastrophic flood of the Mediterranean after the Messinian salinity crisis. *Nature* 462, 778–781. <https://doi.org/10.1038/nature08555>.
- Gardosh, M.A., Tannenbaum, E., 2014. The Petroleum Systems of Israel. AAPG Special Volumes, Memoir 106: *Petroleum Systems of the Tethyan Region*, pp. 179–216.
- Garziglia, S., Migeon, S., Ducassou, E., Loncke, L., Mascle, J., 2008. Mass-transport deposits on the Rosetta province (NW Nile deep-sea turbidite system, Egyptian margin): characteristics, distribution, and potential causal processes. *Mar. Geol.* 250, 180–198. <https://doi.org/10.1016/j.margeo.2008.01.016>.
- Giresse, P., Loncke, L., Huguen, C., Muller, C., Mascle, J., 2010. Nature and origin of sedimentary clasts associated with mud volcanoes in the Nile deep-sea fan. Relationships with fluid venting. *Sediment. Geol.* 228, 229–245. <https://doi.org/10.1016/j.sedgeo.2010.04.014>.
- Gradstein, F.M., Ogg, J.G., Schmitz, M.D., Ogg, G.M., 2012. *The Geologic Time Scale* 2012, pp. 1–29.
- Grauls, D., Baleix, J., 1994. Role of overpressures and in situ stresses in fault-controlled hydrocarbon migration: a case study. *Mar. Petrol. Geol.* 11, 734–742. [https://doi.org/10.1016/0264-8172\(94\)90026-4](https://doi.org/10.1016/0264-8172(94)90026-4).
- Gulmammadov, R., 2017. *Seismic Geomechanics of Mud Volcanoes*. The University of Manchester.
- Halim, M., Said, M., El Azhary, T., 1996. The geochemical characteristics of the Mesozoic and tertiary hydrocarbons in the western desert and Nile delta basins—Egypt. In: 13th Egyptian General Petroleum Corporation Exploration and Production Conference, 21–24 October 1996, Cairo, Egypt, pp. 401–416.
- Hammond, A.L., 1974. Bright spot: better seismological indicators of gas and oil. *Science* 185, 515–517.
- Hanafi, S., Nimmagadda, S.L., Mahmoud, S.E., Mabrouk, W.M., Farhood, K., 2016. Regional integrated interpretation of the hydrocarbon prospectivity of the Nile Delta, Offshore Egypt. *Arabian J. Geosci.* 9, 376. <https://doi.org/10.1007/s12517-016-2387-9>.
- Heppard, P.D., Albertin, M.L., 1998. Abnormal pressure evaluation of the recent Pliocene and Miocene gas discoveries from the Eastern Nile Delta, Egypt, using 2D and 3D seismic data. *Houst. Geol. Soc. Bull.* 41, 16–17, 19, 21, and 23.
- Hsu, K.J., Montadert, L., Bernoulli, D., Cita, M.B., Erickson, A., Garrison, R.E., Kidd, R.B., Mèlières, F., Müller, C., Wright, R., 1977. History of the Mediterranean salinity crisis. *Nature* 267, 399–403.
- Hubbert, M.K., Willis, D.G., 1957. Mechanics of hydraulic fracturing. *Petrol. Trans. AIME* 210, 153–168. <https://doi.org/10.2118/686-G>.
- Hübscher, C., Cartwright, J., Cypionka, H., Delange, G.J., Robertson, A., Suc, J.P., Urai, J.L., 2007. Global look at salt giants. *Eos, Trans. Am. Geophys. Union* 88, 177–179. <https://doi.org/10.1029/2007EO160002>.
- Hurwitz, S., Manga, M., 2017. The fascinating and complex dynamics of geyser eruptions. *Annu. Rev. Earth Planet Sci.* 45, 31–59. <https://doi.org/10.1146/annurev-earth-063016-015605>.
- Javanshir, R.J., Riley, G.W., Duppenbecker, S.J., Abdullayev, N., 2015. Validation of lateral fluid flow in an overpressured sand-shale sequence during development of Azeri-Chirag-Gunashli oil field and Shah Deniz gas field: south Caspian Basin, Azerbaijan. *Mar. Petrol. Geol.* 59, 593–610. <https://doi.org/10.1016/j.marpetgeo.2014.07.019>.
- Judd, A., Hovland, M., 2009. *Seabed Fluid Flow: the Impact on Geology, Biology and the Marine Environment*, pp. 7–12.
- Kanno, Y., Ichihara, M.J.B.O.V., 2018. Sawtooth wave-like pressure changes in a syrup eruption experiment: implications for periodic and nonperiodic volcanic oscillations. *Bull. Volcanol.* 80, 1–18. <https://doi.org/10.1007/s00445-018-1227-z>.
- Kellner, A., Brink, G., El Khawaga, H., 2018. Depositional history of the western Nile delta, Egypt: late Rupelian to Pleistocene. AAPG (Am. Assoc. Pet. Geol.) Bull. 102, 1841–1865. <https://doi.org/10.1306/02161817234>.
- Kirkham, C., Bertoni, C., Cartwright, J., Lensky, N.G., Sirotta, I., Rodriguez, K., Hodgson, N., 2020a. The demise of a 'salt giant' driven by uplift and thermal dissolution. *Earth Planet Sci. Lett.* 531, 115933. <https://doi.org/10.1016/j.epsl.2019.115933>.
- Kirkham, C., Cartwright, J., 2021. Mud volcanoes and dissolution structures as kinematic markers during salt tectonic deformation. *Basin Res.* <https://doi.org/10.1111/bre.12612>.
- Kirkham, C., Cartwright, J., Bertoni, C., Rodriguez, K., Hodgson, N., 2019. 3D kinematics of a thick salt layer during gravity-driven deformation. *Mar. Petrol. Geol.* 110, 434–449. <https://doi.org/10.1016/j.marpetgeo.2019.07.036>.
- Kirkham, C., Cartwright, J., Bertoni, C., Van Rensbergen, P., 2020b. The genesis of a giant mud canopy by catastrophic failure of a thick evaporite sealing layer. *Geology* 48, 787–791. <https://doi.org/10.1130/G47430.1>.
- Kirkham, C., Cartwright, J., Hermanrud, C., Jebsen, C., 2017. The spatial, temporal and volumetric analysis of a large mud volcano province within the Eastern Mediterranean. *Mar. Petrol. Geol.* 81, 1–16. <https://doi.org/10.1016/j.marpetgeo.2016.12.026>.
- Kirkham, C., Cartwright, J., Hermanrud, C., Jebsen, C., 2018a. The formation of giant clastic extrusions at the end of the Messinian Salinity Crisis. *Earth Planet Sci. Lett.* 482, 434–445. <https://doi.org/10.1016/j.epsl.2017.11.001>.
- Kirkham, C., Cartwright, J., Hermanrud, C., Jebsen, C., 2018b. The genesis of mud volcano conduits through thick evaporite sequences. *Basin Res.* 30, 217–236. <https://doi.org/10.1111/bre.12250>.
- Krijgsman, W., Hilgen, F., Raffi, I., Sierro, F., Wilson, D., 1999. Chronology, causes and progression of the Messinian salinity crisis. *Nature* 400, 652–655. <https://doi.org/10.1038/23231>.
- Lofi, J., Sage, F., Déverchère, J., Loncke, L., Maillard, A., Gaullier, V., Thion, I., Gillet, H., Guennoc, P., Gorini, C., 2011. Refining our knowledge of the Messinian salinity crisis records in the offshore domain through multi-site seismic analysis. *Bull. Soc. Geol. Fr.* 182, 163–180. <https://doi.org/10.2113/gssgfbull.182.2.163>.
- Loncke, L., Gaullier, V., Mascle, J., Vendeville, B., Camera, L., 2006. The Nile deep-sea fan: an example of interacting sedimentation, salt tectonics, and inherited subsalt paleotopographic features. *Mar. Petrol. Geol.* 23, 297–315. <https://doi.org/10.1016/j.marpetgeo.2006.01.001>.
- Loncke, L., Mascle, J., Parties, F.S., 2004. Mud volcanoes, gas chimneys, pockmarks and mounds in the Nile deep-sea fan (Eastern Mediterranean): geophysical evidences. *Mar. Petrol. Geol.* 21, 669–689. <https://doi.org/10.1016/j.marpetgeo.2004.02.004>.
- Løseth, H., Gading, M., Wensaas, L., 2009. Hydrocarbon leakage interpreted on seismic data. *Mar. Petrol. Geol.* 26, 1304–1319. <https://doi.org/10.1016/j.marpetgeo.2008.09.008>.
- Løseth, H., Wensaas, L., Arntsen, B., Hanken, N.-M., Basire, C., Graue, K., 2011. 1000 m long gas blow-out pipes. *Mar. Petrol. Geol.* 28, 1047–1060. <https://doi.org/10.1016/j.marpetgeo.2010.10.001>.
- Luo, X., Vasseur, G., 1996. Geopressuring mechanism of organic matter cracking: numerical modeling. AAPG Bull. 80, 856–873. <https://doi.org/10.1306/64ED88EA-1724-11D7-8645000102C1865D>.
- Luo, X., Vasseur, G.J.B.R., 1995. Modelling of Pore Pressure Evolution Associated with Sedimentation and Uplift in Sedimentary Basins, vol. 7, pp. 35–52. <https://doi.org/10.1111/j.1365-2117.1995.tb00094.x>.
- Macgregor, D.S., 2012. The development of the Nile drainage system: integration of onshore and offshore evidence. *Petrol. Geosci.* 18, 417–431. <https://doi.org/10.1144/petgeo.2011.074>.



- Mandl, G., Harkness, R., 1987. Hydrocarbon migration by hydraulic fracturing. Geological Society, London, Special Publications 29, 39–53. <https://doi.org/10.1144/GSL.SP.1987.029.01.04>.
- Manzi, V., Gennari, R., Hilgen, F., Krijgsman, W., Lugli, S., Roveri, M., Sierro, F.J., 2013. Age refinement of the Messinian salinity crisis onset in the Mediterranean. *Terra Nova* 25, 315–322. <https://doi.org/10.1111/ter.12038>.
- Masclé, J., Mary, F., Praeg, D., Brosolo, L., Camera, L., Ceramicola, S., Dupré, S., 2014. Distribution and geological control of mud volcanoes and other fluid/free gas seepage features in the Mediterranean Sea and nearby Gulf of Cadiz. *Geo Mar. Lett.* 34, 89–110. <https://ezproxy-prd.bodleian.ox.ac.uk:2102/10.1007/s00367-014-0356-4>.
- Meilijon, A., Hilgen, F., Sepúlveda, J., Steinberg, J., Fairbank, V., Flecker, R., Waldmann, N.D., Spaulding, S.A., Bialik, O.M., Boudinot, F.G., 2019. Chronology with a pinch of salt: integrated stratigraphy of Messinian evaporites in the deep Eastern Mediterranean reveals long-lasting halite deposition during Atlantic connectivity. *Earth Sci. Rev.* 194, 374–398. <https://doi.org/10.1016/j.earscirev.2019.05.011>.
- Moss, J., Cartwright, J., 2010a. 3D seismic expression of km-scale fluid escape pipes from offshore Namibia. *Basin Res.* 22, 481–501. <https://doi.org/10.1111/j.1365-2117.2010.00461.x>.
- Moss, J., Cartwright, J., 2010b. The spatial and temporal distribution of pipe formation, offshore Namibia. *Mar. Petrol. Geol.* 27, 1216–1234.
- Mousoliotis, A., Albanakis, K., Georgakopoulos, A., Papatheodorou, G., Tripanas, E., Medvedev, B.J.M., Geology, P., 2020. Pre-salt clastic systems in the Herodotus Basin. *SE Mediterranean Sea* 122, 104691. <https://doi.org/10.1016/j.marpetgeo.2020.104691>.
- Muggeridge, A., Abacioglu, Y., England, W., Smalley, C., 2004. Dissipation of anomalous pressures in the subsurface. *J. Geophys. Res. Solid Earth* 109. <https://doi.org/10.1029/2003JB002922>.
- Nashaat, M., 1994. Abnormally high formation pressure and seal impacts on hydrocarbon accumulations in the Nile Delta and North Sinai basins, Egypt. In: Law, B.E., Ulmishek, G.F., Slavin, V.I. (Eds.), *Abnormal Pressures in Hydrocarbon Environments*, vol. 70. AAPG Memoir, pp. 161–180.
- Needham, D.L., Pettingill, H.S., Christensen, C.J., 2017. The Tamar giant gas field: opening the subsalt Miocene gas play in the Levant Basin. In: AAPG Special Volumes, vol. 113. Memoir, pp. 221–256. <https://doi.org/10.1306/13572009M1133688>.
- Oppo, D., Capozzi, R., Tingay, M., Marabini, S.J.G.R.L., 2021a. Early Burial Mud Diapirism: Lateral Overpressure Transfer and Slope Failure in a Deformed Foredeep, vol. 48, e2021GL094922.
- Oppo, D., Evans, S., Iacopini, D., Kabir, S.M., Maselli, V., Jackson, C.A.-L., 2021b. Leaky salt: pipe trails record the history of cross-evaporite fluid escape in the northern Levant Basin, Eastern Mediterranean. *Basin Res.* 33, 1798–1819. <https://doi.org/10.1111/bre.12536>.
- Osborne, M.J., Swarbrick, R.E., 1997. Mechanisms for generating overpressure in sedimentary basins: a reevaluation. *AAPG Bull.* 81, 1023–1041. <https://doi.org/10.1306/522B49C9-1727-11D7-8645000102C1865D>.
- Pierre, C., Bayon, G., Blanc-Valleron, M.-M., Masclé, J., Dupré, S., 2014. Authigenic carbonates related to active seepage of methane-rich hot brines at the Cheops mud volcano, Menes caldera (Nile deep-sea fan, eastern Mediterranean Sea). *Geo Mar. Lett.* 34, 253–267. <https://doi.org/10.1016/j.jsg.2018.07.016>.
- Price, N.J., Cosgrove, J.W., 1990. *Analysis of Geological Structures*, p. 502.
- Prinzhofer, A., Deville, E., 2013. Origins of hydrocarbon gas seeping out from offshore mud volcanoes in the Nile delta. *Tectonophysics* 591, 52–61. <https://doi.org/10.1016/j.tecto.2011.06.028>.
- Ratner, M., 2016. *Natural Gas Discoveries in the Eastern Mediterranean*. Congressional Research Service, Washington, DC, US, pp. 1–18. Congressional Research Service.
- Roberts, S.J., Nunn, J.A., 1995. Episodic fluid expulsion from geopressed sediments. *Mar. Petrol. Geol.* 12, 195–204. [https://doi.org/10.1016/0264-8172\(95\)92839-O](https://doi.org/10.1016/0264-8172(95)92839-O).
- Roveri, M., Lugli, S., Manzi, V., Gennari, R., Schreiber, B.C., 2014. High-resolution strontium isotope stratigraphy of the Messinian deep Mediterranean basins: implications for marginal to central basins correlation. *Mar. Geol.* 349, 113–125. <https://doi.org/10.1016/j.margeo.2014.01.002>.
- Ryan, W.B., 2009. Decoding the Mediterranean salinity crisis. *Sedimentology* 56, 95–136. <https://doi.org/10.1111/j.1365-3091.2008.01031.x>.
- Ryan, W.B., Cita, M.B., 1978. The nature and distribution of Messinian erosional surfaces—indicators of a several-kilometer-deep Mediterranean in the Miocene. *Mar. Geol.* 27, 193–230. [https://doi.org/10.1016/0025-3227\(78\)90032-4](https://doi.org/10.1016/0025-3227(78)90032-4).
- Said, R., 1962. *The Geology of Egypt*. Elsevier, New York.
- Salem, R., 1976. Evolution of Eocene-Miocene sedimentation patterns in parts of northern Egypt. *AAPG (Am. Assoc. Pet. Geol.) Bull.* 60, 34–64. <https://doi.org/10.1306/83D92280-16C7-11D7-8645000102C1865D>.
- Samuel, A., Kneller, B., Raslan, S., Sharp, A., Parsons, C., 2003. Prolific deep-marine slope channels of the Nile Delta, Egypt. *AAPG Bull.* 87, 541–560. <https://doi.org/10.1306/1105021094>.
- Schoenherr, J., Urai, J.L., Kukla, P.A., Litke, R., Schléder, Z., Larroque, J.-M., Newall, M. J., Al-Abry, N., Al-Siyabi, H.A., Rawahi, Z.J.A.B., 2007. Limits to the Sealing Capacity of Rock Salt: A Case Study of the Infra-cambrian Ara Salt from the South Oman Salt Basin., vol. 91, pp. 1541–1557. <https://doi.org/10.1306/06200706122>.
- Sharaf, L., 2003. Source rock evaluation and geochemistry of condensates and natural gases, offshore Nile Delta, Egypt. *J. Petrol. Geol.* 26, 189–209. <https://doi.org/10.1111/j.1747-5457.2003.tb00025.x>.
- Sriapai, T., Walsri, C., Fuenkajorn, K., 2012. Effect of temperature on compressive and tensile strengths of salt. *Sci. Asia* 38, 166–174. <https://doi.org/10.2306/scienceasia1513-1874.2012.38.166>.
- Stewart, S.A., Davies, R.J., 2006. Structure and emplacement of mud volcano systems in the South Caspian Basin. *AAPG Bull.* 90, 771–786. <https://doi.org/10.1306/11220505045>.
- Tingay, M.R., Morley, C.K., Laird, A., Limpornpipat, O., Krisadasima, K., Pabchanda, S., Macintyre, H.R., 2013. Evidence for overpressure generation by kerogen-to-gas maturation in the northern Malay Basin. *AAPG Bull.* 97, 639–672. <https://doi.org/10.1306/09041212032>.
- Underwood, C.J., King, C., Steurbaut, E., 2013. Eocene initiation of Nile drainage due to East African uplift. *Palaeogeogr. Palaeoclimatol. Palaeoecol.* 392, 138–145. <https://doi.org/10.1016/j.palaeo.2013.09.014>.
- Vandré, C., Cramer, B., Gerling, P., Winsemann, J., 2007. Natural gas formation in the western Nile delta (Eastern Mediterranean): thermogenic versus microbial. *Org. Geochem.* 38, 523–539. <https://doi.org/10.1016/j.orggeochem.2006.12.006>.
- Weijermars, R., Jackson, M.P.J.A.B., 2014. Predicting the Depth of Viscous Stress Peaks in Moving Salt Sheets: Conceptual Framework and Implications for Drilling, vol. 98, pp. 911–945. <https://doi.org/10.1306/09121313044>.
- Willson, S.M., Fredrich, J.T., 2005. Geomechanics considerations for through-and near-salt well design. In: *SPE Annual Technical Conference and Exhibition*. OnePetro.
- Woodside, J., De Lange, G.J., Dupre, S., 2004. MIMES (Multiscale investigations of eastern Mediterranean seep systems). In: *An Expedition on Pelagia 13 June 2004-14 July 2004: a Contribution to the Mediflux Project of Euromargins*.
- Zucker, E., Gvirtzman, Z., Steinberg, J., Enzel, Y., 2020. Salt tectonics in the Eastern Mediterranean Sea: where a giant delta meets a salt giant. *Geology* 48, 134–138. <https://doi.org/10.1130/G47031.1>.